UNIVERSITY OF TARTU

Faculty of Science and Technology

Institute of Technology

Frida Matiyevskaya

S phase cyclin-CDK specificity in ordering cell cycle phosphorylation

Bachelor's Thesis (12 ECTS)

Curriculum Science and Technology

Supervisors:

PhD Ilona Faustova

MSc Mihkel Örd

Tartu 2020

S phase cyclin-CDK specificity in ordering cell cycle phosphorylation

Abstract:

Cell proliferation is an essential process in all organisms. Through a series of growth and division, the cell passes its genetic material to the next generation of cells. The molecular machinery that governs timing and execution of these events is called cyclin-dependent kinase (CDK). CDK is activated by multiple cyclins and phosphorylates hundreds of proteins associated with the cell cycle. The specificity of phosphorylation is partly dictated by recognition sequences on proteins called docking motifs that bind specific cyclins. These docking motifs create a plethora of barcodes that allow CDK to recognize and differentially phosphorylate many targets. In this work, a novel S-phase specific docking motif NLxxxL present in CDK inhibitory protein Far1 was mapped and the contribution of cyclin and Cks1 docking on Far1 degradation was analyzed.

Keywords: cell cycle, phosphorylation, cyclin-dependent kinase, cyclin, kinase specificity

CERCS: B230 Microbiology, bacteriology, virology, mycology; P310 Proteins, enzymology

S-faasi CDK spetsiifilisus rakutsükli fosforüleerimise ajastamises

Lühikokkuvõte:

Rakkude jagunemine on hädavajalik, sest see on aluseks geneetilise materjali ülekandeks järgmisesse rakkude põlvkonda. Rakutsüklit reguleerivad tsükliinist sõltuvad kinaasid (CDK), mis fosforüleerivad sadu substraatvalke, mis viivad läbi erinevaid rakutsükli sündmuseid. CDK substraatide fosforüleerimises mängivad olulist rolli tsükliinid, mis seonduvad kindlate motiividega substraatvalkudes. Need motiivid võimaldavad CDK kompleksil erinevatel ajahetkedel rakutsükli jooksul fosforüleerida sadu erinevaid valke. Käesolevas töös kirjeldati uus S-faasi CDK spetsiifiline tsükliin-substraat seondumismotiiv NLxxxL ning uuriti erinevate mehhanismide olulisust substraatide fosforüleerimisel.

Võtmesõnad: rakutükkel, fosforüleerimine, tsükliinist sõltuv kinaas, tsükliin, kinaasi spetsiifika

CERCS: B230 Mikrobioloogia, bakterioloogia, viroloogia, mükoloogia; P310 Proteiinid, ensümoloogia

TABLE OF CONTENTS

TERMS, ABBREVIATIONS AND NOTATIONS

APC - Anaphase promoting complex

CAK1 - Cyclin-dependent kinase activating kinase

CDK - Cyclin-dependent kinase

CKI - Cyclin-dependent kinase inhibitor

EDTA - Ethylenediaminetetraacetic acid

EGFP - Eukaryotic green fluorescent protein

IPTG - Isopropyl β- d-1-thiogalactopyranoside

LB - Luria-Bertani media

LP - Leucine- and proline-rich docking motif for Cln1/2-Cdk1

LxF - Clb2-Cdk1 docking motif

MAP - Mitogen-activated protein

OD600 - Optical density at 600 nm

ORC - Origin recognition complex

RxL - S-CDK docking motif

SC - Synthetic complete media

SC-URA - Synthetic complete media lacking uracil

SCF - Skp1, Cullin, F-box protein containing complex

SDS-PAGE - Sodium dodecyl sulfate polyacrylamide gel electrophoresis

SLiM - Short linear interaction motif

SS-DNA - Salmon Sperm DNA

TE - Tris-EDTA

YPD - Yeast extract, peptone, dextrose media

Introduction

Human body contains around 30 trillion cells. Every day nearly two trillion of them divide. This extremely complex and highly regulated process of the cell growth and division is called the cell cycle. The cell cycle consists of four main phases: G1, S, G2 and M. During this series of events, the cell grows, replicates its DNA and then distributes the content to two daughter cells. The disruption of the cell cycle regulation can lead to uncontrolled division, which is the basis of cancer. Thereby, understanding the molecular processes in the cell cycle control is a key step towards designing therapeuticals.

The core cell cycle regulation machinery is conserved in eukaryotes. For this reason, *S. cerevisiae* is widely used as a model organism for cell cycle research. The regulatory machinery that governs the sequential order of all cell cycle events in budding yeast is called cyclin-dependent kinase 1 (CDK1). In order for CDK1 to be active, another molecule called cyclin must bind to it. Multiple cyclins are expressed in waves during the cell cycle and the formed cyclin-Cdk1 complexes coordinate specific events by phosphorylation of hundreds of proteins. In addition to cyclin, a small adaptor subunit Cks1 binds to CDK1 and promotes multisite phosphorylation of substrates. Despite exhaustive research in this field the question of how CDK1 orchestrates the cell cycle remains open.

The periodically expressed cyclins have been found to affect the substrate targeting of Cdk1 by binding to linear motifs on substrates. These docking interactions could target Cdk1 to phosphorylate specific substrates at different cell cycle stages, necessary for proper cell cycle progression. Therefore studying these interactions can give us more insight on how CDK1 activates or inactivates the sheer variety of proteins during the cell cycle.

When a cell receives signals for mating, an inhibitor protein Far1 binds to S-phase cyclin-CDK complex (Clb5-Cdk1) and prevents cell cycle progression. Without mating pheromone, however, Clb5-Cdk1 phosphorylates and inactivates Far1. It was recently discovered that Far1 contains a novel docking motif for cyclin Clb5. The aim of this work is to define the novel cyclin docking motif in Far1 and estimate its globality among other substrates. In addition, the effect of cyclin docking affinity on the timing of substrate phosphorylation is studied.

1 LITERATURE REVIEW

1.1 The Cell Cycle

Life is composed of the most fundamental building blocks of all organisms - cells. Inside each cell, there is a nucleus that stores DNA which contains all of the instructions on how to build an organism. Every cell is the result of quadrillions of cycles of growth and division. The cell cycle is an essential process in all living organisms that helps to transmit genetic information from one generation to another by the means of reproduction, and serves as a basis of growth and development in multicellular organisms. Throughout this complex process, the content of the cell is first duplicated and then distributed to two individual daughter cells.

The cell cycle is generally broken down into four discrete steps: G1, S, G2, and M phases (**Figure 1**). During the first part of the cell cycle, G1 phase, a cell grows and carries out its regular functions. As soon as sufficient cell size is reached and extracellular signals promoting proliferation are present, the cell enters S phase, where DNA is replicated, resulting in duplicated chromosomes. In G2 phase cell continues to grow and prepares itself for the cell division. Finally, in M phase, the cell distributes its components in half, and forms two genetically identical daughter cells (Morgan, 2007).

The two gap phases, G1 and G2, not just provide additional time for cell growth, but also time to sense the internal and external signals to make sure that conditions are suitable and that preparations are complete before committing to the chromosome duplication and segregation phases. The first commitment the cell has to make happens in G1 phase, making G1 especially important. When conditions are unfavourable for growth or inhibitory signals are detected, cells slow down the progress through G1 and may even enter a nondividing state known as *G0* (**Figure 1**). As soon as conditions for proliferation are favorable and signals to grow and divide are present, cells progress through a commitment point, after which it carries out a DNA replication and cell division, despite any negative extracellular signals (Morgan, 2007).

The next major event in the cell cycle is DNA replication that takes place in S phase. Initiation of the DNA synthesis begins at specific sites called replication origins, which are

scattered along each chromosome. The helicase, accumulated in G1, binds to the DNA and unwinds the double helix, allowing other enzymes to synthesise DNA in both directions and produce two identical double strands. Structural proteins called histones then package DNA into two sister chromatids that are later joined together in a chromosome (Fragkos et al., 2015).

Following the completion of DNA replication, the cell enters G2 phase where it continues to grow and prepares itself for division. During M phase, the cell reorganizes all of its components and divides into two individual daughter cells. M phase is divided into two separate stages: mitosis, where the nuclear division of chromosomes occurs, and cytokinesis, where the cell divides into two. Mitosis in turn includes another subdivision: prophase, metaphase, anaphase, and telophase. During prophase nuclear membrane breaks down, chromosomes are condensed by phosphorylation of histones and are separated to the opposite sides of the nucleus by centromeres attached to an array of protein polymers called microtubules. In metaphase the attached chromosomes are aligned at the equatorial plate and in anaphase, the chromosomes are pulled by microtubules to opposite ends of the cell. At the next stage, telophase, the nuclei are formed around separated chromosomes, and during cytokinesis the cell divides its content into two daughter cells (Bavle, 2014).

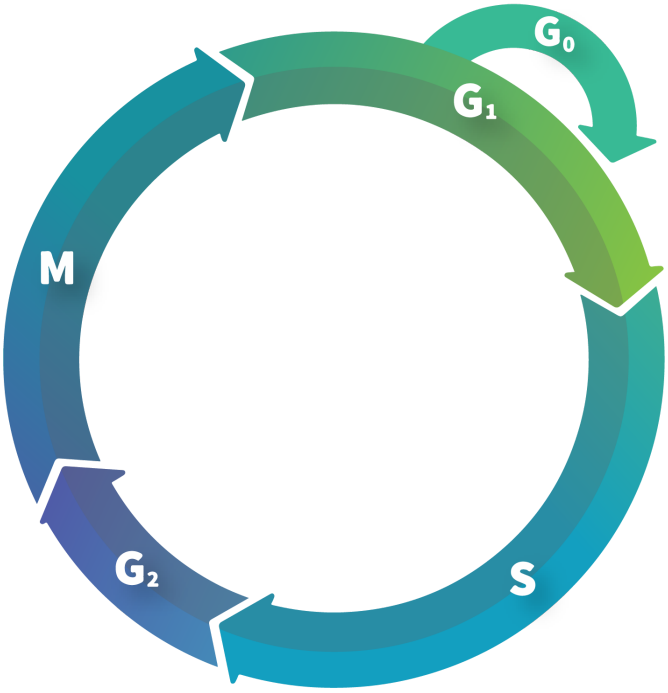

Figure 1. The cell cycle is divided into four phases: G1, S, G2, and M. During two gap phases G1 and G2, a cell grows and accumulates nutrients required for proliferation. In S phase, DNA is replicated, and the genetically identical daughter cells are formed in M phase. Some cells can also enter a non-dividing phase G0 and reside there for long periods of time, eg. fully differentiated neurons (Morgan, 2007).

1.2 Yeast cell cycle control system

Although some properties of the cell cycle, such as the lengths of different phases, differ from species to species, the general organisation and the molecular machinery that governs it, is conserved among eukaryotes (Cross et al., 2011). The clockwork of the cell was first discovered in some of the simplest eukaryotic model organisms such as yeasts (Malumbres and Barbacid, 2005). The budding yeast (*S. cerevisiae*) is an ovoid-shaped fungi cell that has a small genome and cellular architecture similar to higher eukaryotes, such as humans. Since *S. cerevisiae* cells can proliferate in a haploid state, the genome manipulation in this organism is fairly easy. Partially due to the small genome, the budding yeast cells divide rapidly, with the average cell cycle length being around 90 minutes compared to 24 hours in dividing human cells (Cooper, 2000). Taking into account the large amount of data obtained over the years of experimental studies on this microorganism, and the fast development of methodologies for manipulating this species, yeasts are widely used model organisms for investigating the cell cycle mechanisms (Morgan, 2007).

The biochemical timer that directs an extremely ordered process of the cell cycle is called cyclin-dependent kinase CDK (Coudreuse and Nurse, 2010; Swaffer et al., 2016). In budding yeast particularly, the main regulator of the cell cycle is CDK1. As the name suggests, another partnering molecule, called cyclin, must bind to CDK1 in order to activate it. During cell cycle phases different activating cyclins are expressed, and this oscillating expression of cyclins drives the gradual rise in CDK1 activity (Cross et.al., 2002). Cyclin-CDK1 complexes in turn lead to a cascade of phosphate group transfers from ATP to specific amino acid residues in target substrates (Morgan, 2007). In fact, many cell cycle targets contain multiple sites of phosphorylation that are located within intrinsically disordered regions of proteins (Holt et al., 2009; Tyanova et al., 2013). At low cyclin-CDK1 concentrations only a small fraction of target proteins are phosphorylated, but when the CDK complexes surpass critical concentrations, phosphorylated substrates begin to accumulate and promote multi-level regulation of cell cycle events (Swaffer et al., 2016).

During multisite phosphorylation, CDK1 targets proteins at [S/T]PX[K/R] consensus sites, where serine (S) or threonine (T) is followed by proline (P) and a variable amino acid (X), preferably basic, that is accompanied by either lysine (K) or arginine (R) (Songyang et al.,

1994). CDK1 can also target proteins with a minimal consensus site [S/T]P, but at a lower efficiency (Kõivomägi et al., 2011). This post-translational modification, phosphorylation, opens up a range of regulation mechanisms in proteins: from changing their interactions with other proteins, to controlling their activity, stability, and localization (Lim et al., 2014).

In addition to CDK1, which drives reversible phosphorylation of proteins from late G1 to M phase (Morgan, 2007), another regulator of the cell cycle is responsible for cell cycle exit, by inducing proteolysis of regulatory proteins (Lindon, 2008). This guardian of the cell cycle is called anaphase-promoting complex (APC). APC is a molecular machine that, unlike CDK, attaches small protein ubiquitin to the substrates and tags them for degradation by proteasome (Morgan, 2007). When a cell is ready for nuclear division, APC ubiquitinates a protein called securin, that blocks another protein separase, from triggering a cleavage of cohesin that holds together sister chromatids. This leads to segregation of chromosomes. Prior to triggering anaphase, APC also inactivates the no longer needed S-CDK1, followed by inactivation of M cyclin-CDK1 complexes later in anaphase, by tagging cyclins with ubiquitin (Lu et.al, 2014).

An unidirectional process of the cell cycle is the result of oscillation of cell cycle regulators (Figure 2) (Yang and Ferrell, 2013). CDK1 gene expression is stable throughout the cell cycle, its activity, however, increases dynamically from late G1 phase until M phase as more cyclins bind to it (Örd, and Loog, 2019). On the other hand, APC activity starts progressing during the M phase, where it ubiquitinates cyclins, leading to the drop in CDK1 activity necessary for finishing the cell division. In late G1, however, CDK1 phosphorylates APC subunits to inactivate APC, thus enabling accumulation of S and M cyclins again (Ondracka et al.,2016). This oscillating control network orchestrates the robust and correct temporal order of cell cycle events, as well as ensures the forward flow by controlling switches with sharp thresholds (Gérard et al., 2015).

1.3 Cyclin-dependent kinase (CDK)

In budding yeast *S. cerevisiae* there are six different CDKs: Cdk1 (or Cdc28), Pho85, Ctk1, Ssn3, Kin28 and Bur1. Despite this variety, only the first two CDKs, Cdk1 and Pho85, can bind several cyclins to regulate the cell cycle, whilst the other four bind to a single cyclin and function in regulation of transcription (Enserink and Kolodner, 2010). Although Pho85 plays

an important role during stressful environmental conditions, such as returning to growth after starvation (Huang et.al., 2007), the master regulator of the cell cycle remains to be CDK1, as Cdk1 is the only essential CDK and it governs cell cycle events throughout the cell cycle (Morgan, 1997; Mendenhall and Hodge, 1998).

Similar to other protein kinases, CDK1 has two lobes: an amino-terminal (N) lobe containing β sheets and PSTAIRE helix, and a carboxy-terminal (C) lobe that is composed of α helices and has a segment of the active site (**Figure 2**) (Morgan, 2007). The active site cleft, where ATP binds and the phosphate transfer to protein substrate occurs, is sandwiched between these two lobes. In the absence of activating cyclin, T-loop of Cdk1 blocks the entrance to the catalytic cleft. In addition, the key amino acid residues in the active site are disoriented, thus preventing enzymatic interactions with a target protein. Upon the activation of CDK by cyclin, PSTAIRE helix changes its conformation and facilitates rearranging of the amino acids in active cleft (Jeffrey et.al., 1995). At the same time, the T-loop gets phosphorylated by CDK-activating kinase, CAK1, and moves away from the active site exposing the substrate binding region (Ross et al.,2000). Researchers claim that this movement also increases the contact area of cyclin and CDK1, which promotes cyclin-CDK interaction affinity (Kaldis et al.,1996).

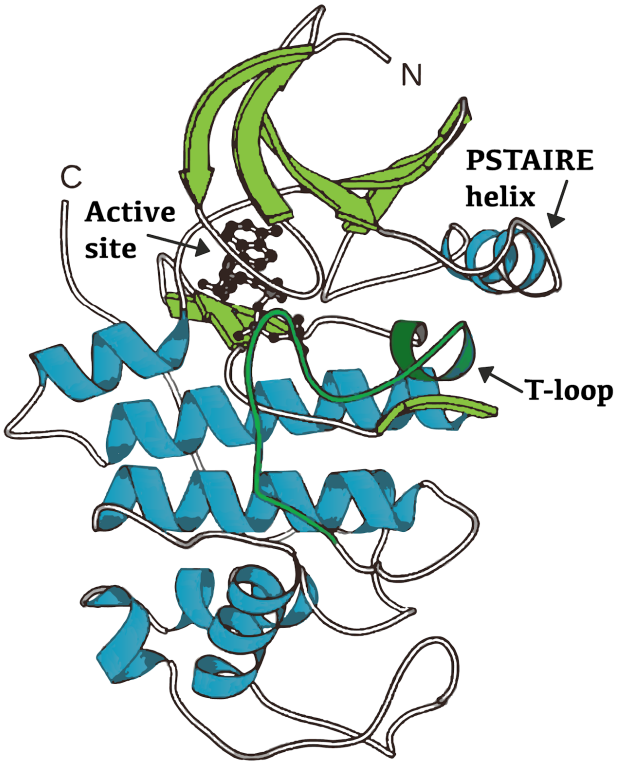

Figure 2. Tertiary structure of CDK1. The main structural components of CDK1 are β sheets (green) and PSTAIRE helix, which form the amino-terminal lobe, and α helices (blue), which make up the carboxy-terminal lobe. The active site of CDK responsible for transferring ATP to the substrate is located between these two lobes. When CDK is inactive, T-loop (dark green) blocks the ATP binding cleft. (This figure was modified from Morgan, 2007)

Once activated by cyclin, CDK1 executes specifically ordered cell cycle events by timely phosphorylation of substrates. To date, there are two mutually inclusive models that describe CDK1 control of the cell cycle. The quantitative model suggests that cell cycle processes are driven by rising CDK1 activity that reaches certain thresholds, as more cyclins bind to it (Swaffer et al., 2016). The qualitative model claims that ordering is achieved by binding of cyclins that are intrinsically different (Örd and Loog, 2019).

1.4 Cyclins

Throughout the cell cycle there are several checkpoints that ensure proper progression conditions. The three major restriction points occur in G1 (Start checkpoint), G2/M and M (metaphase-to-anaphase transition) phases. The transition from one phase to another is mainly driven by multiple CDK activating partners, cyclins, that are expressed at different cell cycle stages (Figure 4). This cell cycle control system generates a robust switch like assembly that ensures correct order of cell cycle events (Bloom and Cross, 2007; Hu and Aparicio, 2005; Schwob and Nasmyth,1993).

Despite their difference in amino acid sequences, cyclins possess similar tertiary structure consisting of α-helices. They also contain a highly conserved region called cyclin box, where CDK binds, as well as a variable hydrophobic patch that targets specific substrates. Two particular subtypes of cyclins that regulate CDK1 in budding yeast are Cln1-3 and Clb1-6 (**Figure 3**). When conditions for proliferation are favorable, Cln3 triggers a cascade of further cyclin expressions (Tyers et al., 1993). First, in late G1 phase Cln3 acts as an upstream regulator and activates transcription of G1/S phase cyclins Cln1 and Cln2. Together these three Cln proteins initiate an irreversible commitment to cell cycle. The rise in Cln1 and Cln2 concentrations stimulates expression of S cyclins Clb5 and Clb6. The latter subsequently results in activation of G2 and M phase cyclins Clb1, 2, 3, and 4 (Wittenberg and Reed, 2005).

The G1 and G1/S Cln1-3 cyclins are mainly responsible for stimulation of the early cell cycle events, such as progression through Start checkpoint, bud formation, duplication of spindle body and most importantly activation of S phase cyclins, by targeting CDK-inhibitor protein

(CKI) Sic1 for degradation. (Morgan, 2007; Yang et al., 2013). Interestingly, experiments in *S. cerevisiae* have shown that only the knockout of all three *CLN* genes is lethal, as otherwise these cyclins can substitute each other in the absence of other Cln proteins (Richardson et al., 1989). Furthermore, unlike other cyclins, Cln3 is constantly expressed during the cell cycle, without oscillations in concentration (Wittenberg et al.,1990). Cln3 expression level, however, has been found to be regulated by environmental conditions, such as nutrient availability (Shi and Tu, 2013). As Cln3 is the most upstream cyclin, regulation of its expression can connect cell cycle entry to growth conditions.

When cyclins Clb5 and Clb6 are activated at the end of G1 phase, they phosphorylate several components of the replication machinery to trigger the initiation of DNA duplication and to ensure that multiple rounds of replication do not occur (Morgan, 2007). The degradation of the two cyclins however is regulated differently. Although CLB5 and CLB6 transcription peaks both rise in the late G1 phase, Clb6 is degraded by SCF complex following G1/S transition (Jackson et al., 2006). Clb5, however, is stable during S, G2 and early mitotic phases, and is degraded in late mitosis by APC destruction complex (Jackson et al., 2006). In spite of experiments showing that Clb5 stimulates efficient DNA replication (Donaldson et al., 1998) and Clb6 inhibits transcription of G1 programs (reference), the functional difference of these two proteins is poorly understood (Morgan, 2007).

The group of G2 cyclins Clb3-4 and M cyclins Clb1-2 are expressed in mid and late S phase respectively and both decline in anaphase, allowing the cell to initiate mitotic exit (Fitch et.al., 1992). Clb1-4 cyclins promote mitotic events, such as spindle assembly, the distribution of sister-chromatids on the spindle and nuclear division (Rahal and Amon, 2008). Previous studies on this subclass of cyclins have shown that single deletions of these genes were viable, whereas any combination with *clb2* deletion was lethal. The cells having only *CLB2* could proceed throughout the cell cycle, with a delayed mitotic entry, indicating that Clb2 could function alone in the absence of other late Clb cyclins (Fitch et.al., 1992).

Nonetheless, the different studies show that cyclins have partially overlapping functions, which makes it difficult to point out the specific role of each (Bloom and Cross, 2007). These differences and overlaps may arise from the substrate targeting mechanisms of the cyclin-CDK complex. All cyclin-Cdk1 complexes share the catalytic subunit, giving rise to

some overlap in specificity. The order of phosphorylation events, however, does not depend solely on the active site of CDK1. In fact, distal interaction of hydrophobic patch in the cyclin and a short docking motif in the substrate, can contribute both to specificity and phosphorylation efficiency. These specific docking interactions have been found to be especially important for early cyclin-CDK complexes (Kõivomägi et al., 2011).

Besides providing specificity in substrate interactions, cyclins can act as scaffold proteins that direct CDK1 to distinct subcellular locations (Morgan, 2007). More specifically, the hydrophobic patch in cyclins is required for CDK1 localization in certain cellular compartments for phosphorylation of M phase targets (Basu et al., 2020).

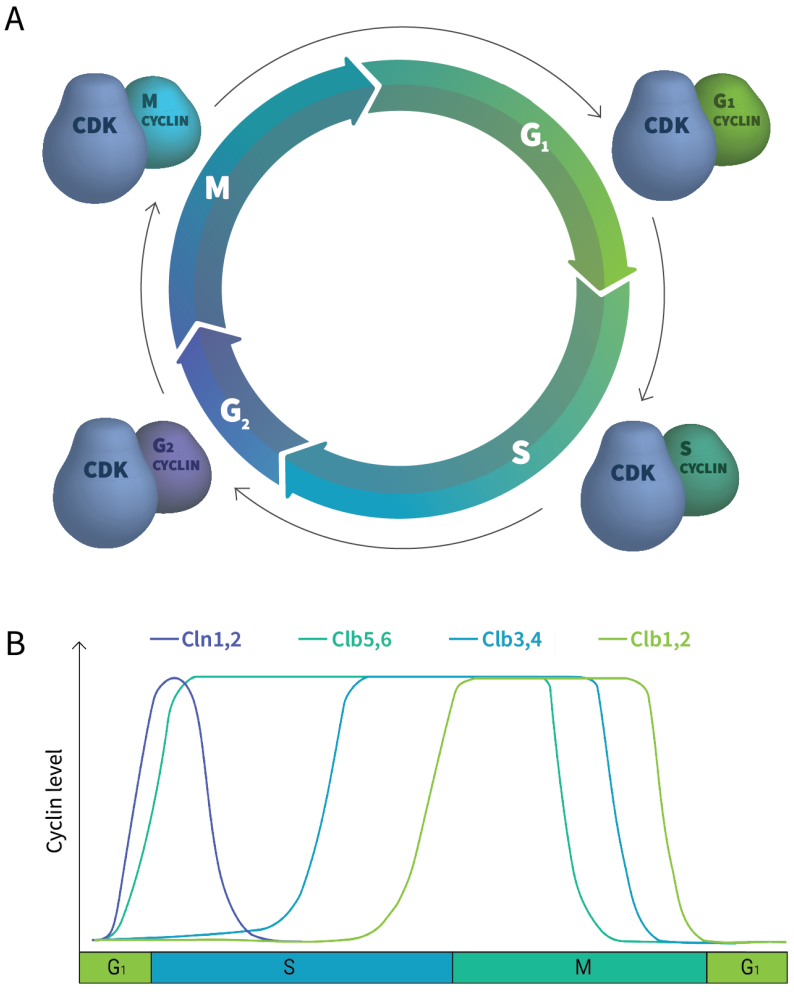

Figure 3. Expression of cyclins during the cell cycle. Specific cyclins are expressed in different cell cycle phases. The figure shows the expression profiles of budding yeast Cdk1 cyclins.

1.5 Cks1

In addition to the cyclin that acts not only as an activator of CDK1 but also as a modulator of substrate specificity and subcellular localization (Bloom and Cross, 2007), the CDK1 complex requires association of an adaptor subunit Cks1 (Pines, 1996). Cks1 mainly serves as an extension of substrate-binding surface that promotes multisite phosphorylation of substrates by CDK1 (Kõivomägi et al., 2011; McGrath, 2013).

Crystal structure of this phosphoadaptor revealed that Cks1 contains a cationic pocket that efficiently binds to phosphorylated threonine that is followed by proline [pTP] (Kõivomägi et al., 2013; McGrath, 2013). After CDK1 or potentially a different kinase phosphorylates a TP site in the protein, Cks1 can bind this priming site and enhance phosphorylation at other sites (Kõivomägi et al., 2013; McGrath, 2013). The distance between Cks1 priming site and CDK1 phosphorylation sites within intrinsically disordered polypeptide chain has been found to affect the rate of Cks1-enhanced phosphorylation (Kõivomägi et al., 2013). Therefore, Cks1 docking interactions play a major role in stimulating cascades of multisite phosphorylation of substrates. Multisite phosphorylation of Cdk1 inhibitor Sic1, for example, occurs via Cks1 docking to achieve phosphorylation of over 6 sites (Kõivomägi et al., 2011).

Previous studies suggest that deletion Cks1 drastically affects the phosphorylation rate of proteins in *Xenopus* egg extracts, suggesting that this subunit promotes multisite phosphorylation also in higher eukaryotes (Patra et al.,1999). For example, multisite phosphorylation of Wee1 and Cdc25 that regulates a mitotic entry has been shown to depend on Cks1 (Patra et al.,1999; Patra and Dunphy, 1998), however little research has been done in that field.

1.6 Cyclin-specific substrate docking motifs

The cyclin-CDK1-Cks1 complex sequentially phosphorylates hundreds of proteins that trigger cell cycle events (Enserink and Kolodner, 2010). Some substrates, however, are only phosphorylated at specific timepoints. The signaling proteins Ste5 and Ste20 in the pheromone pathway, for example, are only targeted when G1/S cyclin binds Cdk1, but not

when Cdk1 is activated by any other cyclins (Bhaduri and Pryciak, 2011). This indicates that cyclin-specific substrate targeting contributes to the order of cell cycle events.

There are many variable docking motifs found in Cdk1 substrates that enhance cyclin-specific interactions. The two previously mentioned proteins Ste5 and Ste20 have a leucine/proline-rich sequence motif [LP] that interacts with Cln1 and Cln2-CDK1 complexes and promotes phosphorylation of CDK consensus sites. Ste5, a MAP kinase scaffold protein, amplifies the pheromone pathway signals that initiate cell cycle arrest before mating. The Cln-Cdk1 mediated phosphorylation of this protein blocks its signal transduction functions and sends it for ubiquitination by SCF ligase that subsequently marks it for degradation by the proteasome (Bhaduri and Pryciak, 2011).

Another set of S phase Cdk1 substrates have a highly conserved recognition motif called RxL that is targeted by Clb5 and Clb6 cyclins (Morgan, 2007). S-phase docking motif RxL has a consensus sequence of K/R-x-L-x-φ or K/R-x-L- φ, where lysine (K) or arginine (R), are followed by a variable amino acid (x), that is flanked by leucine (L), and/or another variable amino residue (x) and a large hydrophobic amino acid (φ) (Lowe et al., 2002). In G1 phase, when CDK activity is absent, a large protein apparatus called origin recognition complex (ORC) binds to DNA and recruits other replication proteins (Morgan, 2007). Orc6 subunit contains an RxL docking motif that interacts with Clb5 hydrophobic patch (Wilmes et al., 2004). This interaction in turn enhances phosphorylation to inhibit ORC binding to the origins, and ultimately protects origins from re-replication. Another interesting example is the cyclin-dependent inhibitor (CKI), Sic1, that in addition to LP docking motif has the S phase cyclin recognition sequence, RxL (Kõivomägi et al., 2011). For successful S phase entry, Sic1, which binds tightly and inhibits Clb5-Cdk1, must be degraded by the SCF complex. The phosphorylation that tags Sic1 for degradation is initiated by Cln1- and Cln2-CDK1 complexes that recognise LP docking motif, and completed by activated Clb5-CDK that use RxL docking for full phosphorylation of Sic1 (Kõivomägi et al., 2011).

Interestingly, the recognition sequences of M phase substrates remained undiscovered for a long time, until recent findings by Örd *et. al*. To identify the conserved docking motif of mitotic Clb cyclins researchers used several mutated versions of Cdc6, a component of pre-replicative complex that inhibits origin re-licensing. By introducing mutations to this

replication factor, scientists found a linear docking motif LxF that increased the rate of substrate phosphorylation by M-CDK1. Further sequence alignment and functionality assessment of the motif in M-phase targets have shown high conservation of the LxF motif, supporting the importance of a novel M-CDK1 specific cyclin docking sequence (Örd et al., 2019).

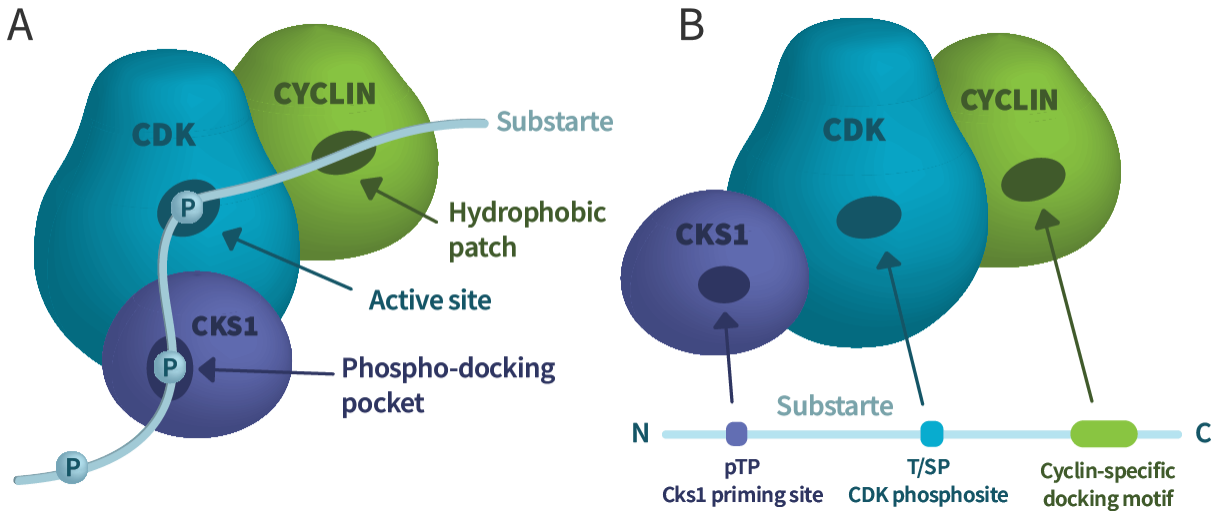

Figure 4. Multisite phosphorylation of substrates by Cyclin-CDK-Cks1 complex. Three main interactions contribute to CDK substrate recognition. The hydrophobic patch of cyclins bind to cyclin-specific docking motifs. The active site interacts with T/SP phosphorylation sites. Cks1 contains a phospho-docking pocket that binds already phosphorylated TP sites.

In addition to providing docking interfaces for the substrates, different cyclins also introduce different activity levels to the kinase active site. The activity of cyclin-Cdk1 complexes towards substrates that do not contain any cyclin docking motifs increases in the order of cyclin appearance in the cell cycle. This prevents premature initiation of mitosis, by providing a time delay needed for accumulation of mitotic phosphorylation (Kõivomägi et al., 2011). On the other hand, early CDK1 complexes can compensate for the otherwise weak intrinsic activity by using docking sites that are specific for the hydrophobic patches in these cyclins (Kõivomägi et al., 2011). These results suggest that docking motifs can be switched in substrates to enhance specificity towards certain cyclins that drive phosphorylation-dependent order of the cell cycle. As described above, the phosphorylation of substrates is determined by three key interactions: active site of CDK1 and consensus site

on the substrate, hydrophobic patch on cyclin and specific docking motif on target protein, and phosphate-binding pocket on Cks1 and substrate priming site (**Figure 4**) (Kõivomägi et al., 2011). Together with continuously increasing CDK1 activity during the cell cycle, these interactions form a highly interconnected plethora of networks that generate robust molecular signals and drive all cell cycle events in a precise and coordinated manner.

1.7 Inhibitory substrate Far1

Haploid *S. cerevisiae* cells secrete and recognize short peptide pheromones. Upon binding of the pheromones from the opposite mating type to the cell surface receptor, a signal transduction pathway activates cell cycle arrest in G1 to prepare the cells for mating. Only G1 cells that have not passed Start checkpoint respond to pheromone. The cell cycle arrest is achieved by activity of cyclin-dependent kinase inhibitors (Vogt and Reed, 1998).

Far1, which stands for factor arrest resistant, is the first discovered CKI that activates cell cycle arrest upon mating (Chang and Herskowitz, 1990). When pheromone signals are present, a mitogen-activated protein (MAP) kinase homologue Fus3 phosphorylates Far1 at T306 residue and initiates its cyclin inhibiting activity (**Figure 5**) (Peter et al., 1993; Pope et al., 2014). In G1 arrest, Far1 suppresses G1/S cyclins activity by outcompeting Cln-CDK1 substrates with its high affinity binding to the substrate docking pocket on these cyclins (Pope et al., 2014). The mechanism by which Far1 inhibits the S phase CDK, however, is not yet known.

When extracellular mating pheromones signals are absent, Far1 is phosphorylated at the S87 and S91 residues and targeted for degradation by the SCF complex (**Figure 5**) (Doncic et al., 2015). Strikingly, recent findings indicate that the protein is phosphorylated by the Clb5-Cdk1 complex, rather than Cln2-Cdk1 (manuscript in supplementary). It was shown that Clb5-CDK1 complex targets the N-terminal region of Far1, although the protein does not contain S-cyclin specific docking motif RxL (manuscript in supplementary). These findings suggest that Far1 may possess another yet unknown S-cyclin specific docking motif that regulates phosphorylation rate of Far1.

Far1 has the length of 830 amino acids, and as many substrates found in the cell, the protein possesses multiple sites of phosphorylation. The first 150 amino acids of Far1 constitute an

intrinsically disordered region that contains eight Cdk1 phosphorylation sites. It has been found that mutation of phosphorylation sites S87 and S91, that form a di-phosphodegron, disrupted the degradation of Far1, indicating that phosphorylation of the degron is needed to tag the protein for degradation (manuscript in supplementary).

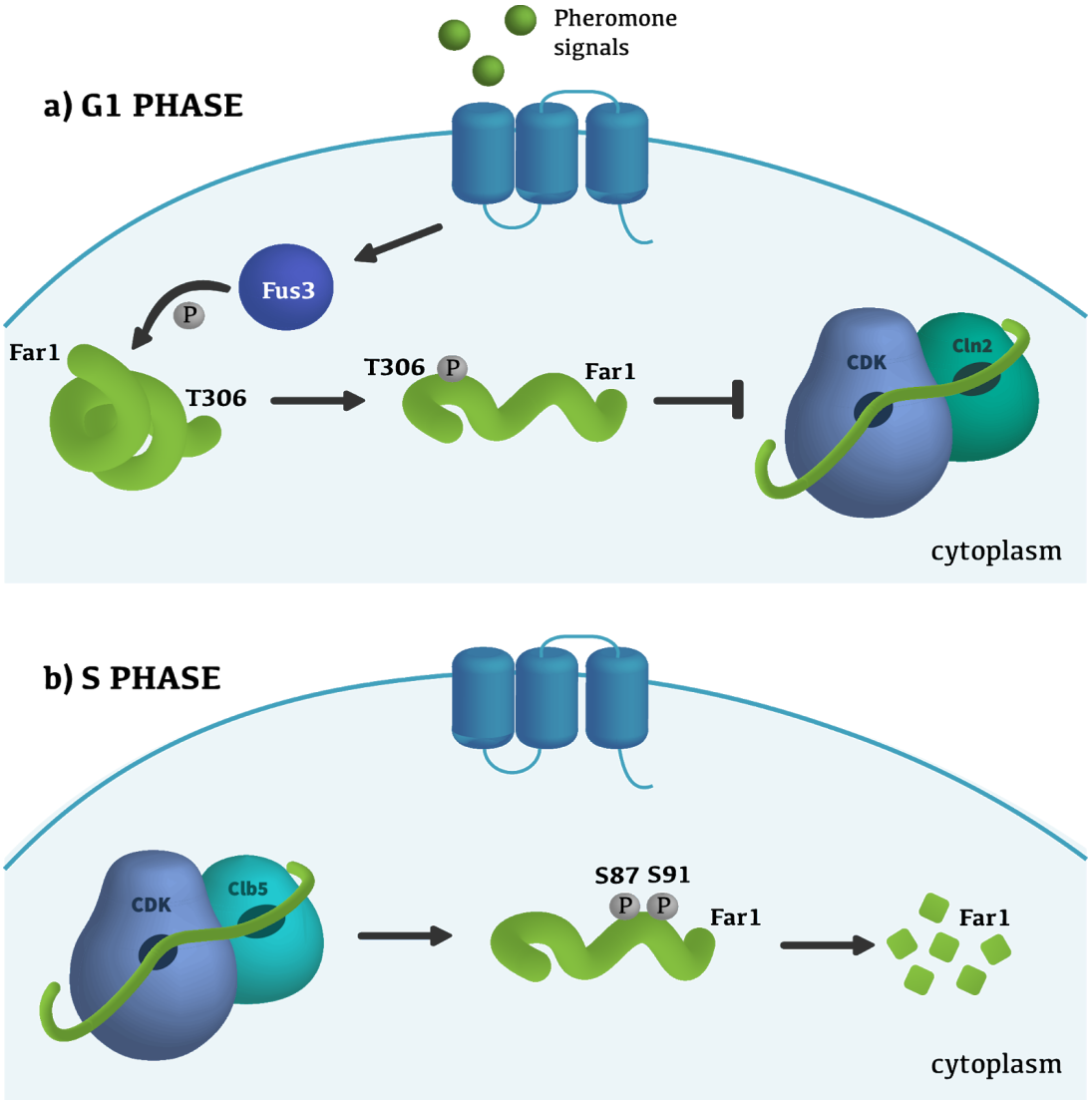

Figure 5. Pheromone signalling activates inhibitory protein Far1. (a) In G1 phase, Far1 can be activated by presence of mating pheromones by Fus3-mediated phosphorylation of T306 in Far1. This leads to inhibition of Cdk1 activity and cell cycle arrest in G1. **(b)** Upon entry to S phase, Far1 is phosphorylated by Clb5-Cdk1 on the S87 S91 degron, which triggers Far1 degradation.

Interestingly, when screening Far1 homologs in different yeast species, researchers found several conserved amino acids in the 130-138 region and they showed that this region exhibits Clb5 binding specificity (manuscript in supplementary). More precisely, leucines in positions 131,135 and 136 appeared to be the most conserved residues, and when the triple alanine mutation was introduced, the degradation of Far1 during the cell cycle was substantially delayed compared to the wild-type. Moreover, when a single leucine at position 135 was substituted with alanine (L135A), a similar delay in degradation as with the triple mutant (L131A, L135A, L136A) was observed. These findings indicate two things: first, the 130-138 region could function as a Clb5-specific linear docking motif, and second, the conserved leucines are important in mediating interaction with Clb5 cyclin (manuscript in supplementary). Although the region contributing to the docking has been mapped, the mechanism of this interaction is still not fully understood.

2 THE AIMS OF THE THESIS

S phase CDK specificity is known to be governed by RxL docking motifs, however, recent work revealed that Far1 contains a region responsible for high Clb5-specificity, but does not contain an RxL motif. This revealed that the S phase substrate targeting could be mediated by additional cyclin docking motifs. To understand this in more detail, the aim of this work is to map the interaction and to compare its properties with the RxL motif.

The specific aims of this thesis are:

1) Define the S-CDK (Clb5) docking motif in Far1;

2) Estimate the globality of the Far1 docking motif among S phase targets;

3) Analyze how different cyclin docking motifs without and in combination with Cks1 docking contribute to the phosphorylation time in the cell cycle.

3 EXPERIMENTAL PART

3.1 MATERIALS AND METHODS

3.1.1 Materials

Following materials and media were used for the experiments.

DNA cloning:

1) 1% agarose TAE gel: 1 mM ethylenediaminetetraacetic acid (EDTA), 5 µl/l Atlas ClearSight DNA Stain (BioAtlas), 40 mM Tris-acetate pH 8.3 and 1% agarose;
2) TAE buffer: 40 mM Tris-acetate pH 8.3 and 1 mM EDTA;
3) LB media: 5 g/l yeast extract (Formedium), 10 g/L NaCl (Chempur) and 10 g/l tryptone (Formedium);
4) LB agar plates with ampicillin or kanamycin: LB media, 15 g/l bacto agar (Formedium), 100 µg/ml ampicillin (Sigma) or 100 µg/ml kanamycin (Sigma);
5) LB agar plates with kanamycin and chloramphenicol: LB media, 15 g/l bacto agar (Formedium), 100 µg/ml kanamycin (Sigma) and 50 µg/ml chloramphenicol (Sigma).

Yeast transformation:

1) YPD media: 20 g/l glucose (Oriola), 10 g/l yeast extract (Formedium) and 20 g/l peptone (Formedium);
2) YPD plates: YPD media and 15 g/l bacto agar (Formedium);
3) 1x TE buffer: 10 mM Tris hydrochloride (Tris-HCl) pH 8 and 1 mM EDTA;
4) PL1 buffer: 100 mM Lithium Acetate dissolved in 0.5 x TE buffer;
5) PL2 buffer: 40% Polyethylene glycol (PEG) 3350, 100 mM Lithium Acetate, 10 mM Tris-HCl pH 8, 1 mM EDTA;
6) SC-URA glucose agar plates: 20 g/l glucose (Oriola), 20 g/l bacto agar (Formedium), 2 g/l SC-URA powder (MP Biomedicals), 7 g/l yeast nitrogen base without amino acids (BD Biosciences).

Time-lapse microscopy:

1) Synthetic complete media (SC) with 2% glucose: 20 g/l peptone (Formedium), 10 g/l CSM (Formedium), 20 g/l glucose (Oriola).
2) 1.5% SC/glucose-agarose gel pad: 20 g/l peptone (Formedium), 10 g/l CSM (Formedium), 20 g/l glucose (Oriola), 1.5% NuSieve GTG agarose (Lonza).

Protein purification:

6) Lysis buffer: 50 mM Tris-HCl pH 7.4, 5% glycerol, 0.1 u/µl DNase, 300 mM NaCl and 1% Triton-X100;
7) Protease inhibitors: 1 mM phenylmethylsulfonyl fluoride (PMSF), 1 µg/ml pepstatin A, 1 µg/ml aprotinin, 1 µg/ml leupeptin;
8) Elution buffer: 50 mM Tris-HCl pH 7.4, 150 mM NaCl, 0.1% NP-40, 5% glycerol, 200 mM imidazole;
9) Buffer B: 50 mM Tris-HCl pH 7.4, 5% glycerol, 0.1 u/µl DNase, 600 mM NaCl and 1% Triton-X100;
10) Buffer C: 50 mM Tris-HCl pH 7.4, 5% glycerol, 0.1 u/µl DNase, 300 mM NaCl, 1% Triton-X100 and 10 mM imidazole.

Kinase assay:

1) 5x kinase buffer (5xKB): 250 mM Hepes-KOH (pH 7.4), 750 mM NaCl, 25 mM $MgCl_2$, 2.5 mM ATP;
2) Sodium dodecyl sulfate (SDS) loading buffer: 60 mM Tris-HCl pH 6, 8.2% SDS, 10% glycerol, 5% β-mercaptoethanol, 0.01% bromophenol blue;
3) SDS–polyacrylamide (SDS-PAGE) separating gel: 0.375 M Tris-HCl (pH 8.8), 10% acrylamide [29:1 acrylamide:bis-acrylamide], 0.1% SDS;
4) SDS-PAGE stacking gel: 0.125 M Tris-HCl (pH 6.8), 5% acrylamide [29:1 acrylamide:bis-acrylamide], 0.1% SDS);
5) SDS-PAGE running buffer: 25 mM Tris, 192 mM glycine, 0.1% SDS.

3.1.2 DNA cloning

The plasmids constructed during this study are presented in Table 1. To obtain the inserts for constructs 1-18 in Table 1, PCR mutagenesis was employed. The procedure included two

rounds of PCR, one for introducing mutations, another for adding a restriction site. Prior to plasmid cloning, PCR primers were designed *in silico* using Benchling (www.benchling.com). Inserts in 1-14 constructs were cloned with *BamHI* restriction site at 5'-end and *SmaI* restriction site at 3'-end to pRS306 vectors containing *SIC1* promoter (1-420 upstream of SIC1) and C-terminal EGFP (eukaryotic green fluorescent protein) coding sequence. The obtained plasmids were later integrated into the yeast genome by homologous recombination and cells containing these mutations were analysed in fluorescent microscopy experiments. The inserts of constructs 15-20 were cloned to pET28a backbone vectors, transformed to *E. coli* BL21 cells and used for protein purification.

The Lif1(nlxxxl) mutation in construct 20 was obtained by overlap-extension PCR. Two target fragments were first separately amplified with overlapping primers in PCR. The obtained products were purified and mixed together in a third PCR, where they were spliced into one fragment via complementary sequences of primers.

Table 1. Plasmids used in this study. Each row in the table contains the name of the plasmid where the insert was integrated, the backbone vector, and restriction sites used for cloning.

Description	**Backbone vector**	**Restriction sites**
Psic1-SV40-Far1(1-150 L131A)-EGFP	pRS306	BamHI/AfeI and SmaI
Psic1-SV40-Far1(1-150 L136A)-EGFP		
Psic1-SV40-Far1(1-150 N130A)-EGFP		
Psic1-SV40-Far1(1-150 resi)-EGFP		
Psic1-SV40-Far1(85-150 MunI)-EGFP		
Psic1-SV40-Far1(85-150 MunI RxL)-EGFP		
Psic1-SV40-Far1(85-150 MunI lxxxll)-EGFP		
Psic1-SV40-Far1(T3+85-150 MunI lxxxll)-EGFP		
Psic1-SV40-Far1(T3+85-150 MunI RxL)-EGFP		

Psic1-SV40-Far1(T3+85-150 MunI)-EGFP	pRS306	BamHI/AfeI and SmaI
Psic1-SV40-Far1(1-150 SP T129K)-EGFP		
Psic1-SV40-Far1(1-150 SP RNLF)-EGFP		
Psic1-SV40-Far1(1-150 SP PKKLQF)-EGFP		
Psic1-SV40-Far1(1-150 SPPRKLQF)-EGFP		
6xHis-SV40-Far1(1-150 N130A)-EGFP	pET28a	BamHI/AfeI and SalI
6xHis-SV40-Far1(1-150 L131A)-EGFP		
6xHis-SV40-Far1(1-150 L135A)-EGFP		
6xHis-SV40-Far1(1-150 L136A)-EGFP		
6xHis-Lif1		NcoI and XhoI
6xHis-Lif1(nlxxxl)		

3.1.2.1 PCR

PCRs were performed using Thermo Scientific Phusion High-Fidelity DNA Polymerase and oligonucleotides from Microsynth. Reactions were carried out according to manufacturers' instructions. When the PCR program was completed the products were separated by gel electrophoresis. This was done by adding 6X Orange DNA Loading Dye (Thermo Scientific) to the PCR mixture and loading it onto a 1% agarose gel. The DNA products were visualized under UV, excised from the gel and purified using FavorPrep GEL/PCR Purification Kit (Favorgen) according to the manufacturer's protocol.

3.1.2.2 Restriction

For the PCR product to be inserted into the target vector, both DNA fragment and backbone vector were restricted with FastDigest enzymes (Thermo Scientific) as shown in Table 1 according to manufacturer's instruction. In addition, the restriction mixture of the vector contained 1 µl of FastAP Thermosensitive Alkaline Phosphatase. FastAP allowed removal of

phosphate groups from restriction sites, thus preventing backbone vector recircularization during ligation.

3.1.2.3 Ligation

The last step of making recombinant plasmid is ligation of the linearized vector and the restricted insert. For that, a mixture containing a 3:1 molar ratio of insert and vector, 1 µl of T4 ligase buffer, 1 µl of T4 ligase (Thermo Scientific) and water to a final volume of 10 µl was incubated at 16 °C for at least 2 hours. When restricted with SmaI, an enzyme that produces blunt ends, 1 µl of 50% polyethylene glycol (PEG) 4000 was added to the ligation mixture. PEG is a hydrophobic molecule that occupies most of the space in the mixture, increasing the likelihood of the blunt-end ligation.

3.1.2.4 Transformation

Following ligation, plasmids were transformed into *E. coli* DH5a cells. For protein expression, the plasmids extracted from DH5a cells were transformed to *E. coli* BL21 cells. The competent cells (stored at -80 ^{o}C) were thawed on ice. For transformation, 50 µl of bacterial cells were suspended with 2 µl of ligation mixture (DH5a) or plasmid DNA (BL21) and chilled on ice for additional 30 minutes. Afterwards, cells were exposed to 42 ^{o}C heat shock for 45 seconds. Next, BL21 and DH5a cells were cooled down on ice for at least five minutes. Subsequently, 500 µl LB media was added to the mixture and incubated for 30-60 minutes at 37 °C in 220 rpm shaker. The cells were centrifuged for 1 minute at 6000 rpm. Most of the supernatant was poured away, leaving only about 200 µl in which the cell precipitate was suspended, and the suspension was plated. DH5a cells were sown on LB agar plates with ampicillin or kanamycin, depending on the vector, while BL21 cells were plated on LB agar plates containing kanamycin and chloramphenicol. The plates were incubated at 37 °C for 12-16 hours.

3.1.2.5 Colony screening

The individual colonies from the transformation plates were picked and incubated overnight in the 5 mL of LB media with 100 µg/mL of ampicillin or kanamycin. After incubation, plasmid DNA from the cells was isolated using FavorPrep Plasmid DNA Extraction Mini Kit

(Favorgen) according to the manufacturer's protocol. To check whether the amplified plasmids corresponded to the correct sizes of cloning vector and insert, the extracted DNA was restricted with FastDigest enzymes (Thermo Scientific) as shown in Table 1. The mixtures were run on 1% agarose gel and visualised under UV light. Then DNA concentration was quantified in the NanoDrop 1000 Spectrophotometer (Thermo Fisher) following the manufacturer's instructions. To validate gene mutations, samples were sent for Sanger DNA sequencing (Estonian Biocentre).

3.1.3 Yeast transformation

For the microscopy experiments, the pRS306-based vectors were transformed to *S. cerevisiae* strain RV298 (*leu2-3,112 trp1-1 can1-100 ura3-1 ade2-1 his3-11,15 [phi+] bar1::hisG WHI5-mCherry-SpHIS5*). About 1 µg of the plasmids were linearized with Eco147I FastDigest enzyme (Thermo Scientific) according to manufacturer's instructions before the transformation.

Before the transformation, RV298 cells were streaked on a YPD plate and incubated overnight at 30 °C. Next day, the culture was transferred from the plate to 50 mL of YPD media and grown at 30 °C in a 160 rpm shaker. As soon as OD600 reached 0.6-0.8, culture was centrifuged for 1 min at 3100 rpm. After centrifugation the supernatant was discharged and the pellet was resuspended in 1 ml of sterile buffer PL1. The mixture was centrifuged again at 3600 rpm for 60 seconds. After removal of the supernatant, a PL1 buffer was added in a ratio of 2:1 to the cell volume and the mixture was incubated at room temperature for 10 minutes. At the same time Salmon Sperm DNA (SS-DNA) was boiled for 10 minutes at 100 °C and cooled down in an ice bath. Afterwards, 100 µl of the competent yeast cells were mixed in a 1.5 µl tube with the linearized plasmid and SS-DNA.

Next step included an addition of 700 µl of sterile buffer PL2 and 48 µl of DMSO, gentle resuspension of the mixture and incubation at 42 °C for 40 minutes. Following incubation, cells were cooled down on ice for 2 minutes, centrifuged for 30 seconds at 6000 rpm and the pellet was resuspended in 1 ml of 1x TE buffer. After that the mixture was again centrifuged for 60 seconds at 3600 rpm, resuspended in 200 µl of 1x TE buffer, plated on SC-URA glucose agar plates and incubated at 30 °C for 2 days.

3.1.4 Microscopy

Since pRS306 vectors can also integrate in multiple copies into the yeast genome, prior to the experiment, yeast cells were screened for the levels of GFP fluorescence signal. Colonies containing one copy of the integrated vector were further separately inoculated in a 3 ml SC media and grown overnight at 30 °C in 160 rpm shaker to the logarithmic growth phase. Following incubation, tubes with cells were vortexed to prevent cells clumping, and 0.3 µl of the mixture was used for the time-lapse experiment. The cells were placed on a 24 x 50 mm glass plate and covered with a 1.5% SC/glucose-agarose gel pad. A 20 x 20 mm micro glass and a small plastic cover were placed on top to prevent gel pieces from moving and drying out.

Fluorescent imaging was performed using a Zeiss Observer Z1 microscope equipped with AxioCam 506 mono-camera and 63x/1.4NA objective. On average, each experiment was 8 hours long, during which no more than 12 positions were imaged every 3 minutes using automated ZEN software and 3x3 binning. Definite Focus was utilised to eliminate focus drift in images. Reporter proteins EGFP and mCherry were excited with Colibri 470 LED and Colibri 540-580 LED modules, set at 15 ms and 750 ms exposure times, respectively. During the whole experiment the temperature of agarose gel was kept at constant 30 °C. Image analysis was performed using MATLAB software (The MathWorks, Inc.). Cell tracking, image segmentation and quantification were performed with supplemented MATLAB code by (Doncic et al., 2013). In the analysis, the cells were synchronized by the time of nuclear export of 50% of Whi5-mCherry. The plots show mean fluorescence values with SEM error bars from a population of cells over the time of the cell cycle. In the analysis of 50% degradation timing, the medians of different constructs are compared to the wild-type in a pair-wise manner using Mann-Whitney U test. On the plots, **** denotes p-value <0.0001, *** <0.001, ** <0.01, *<0.05 and ns > 0.05.

3.1.5 Protein purification

To purify recombinant proteins, immobilized metal-affinity chromatography (IMAC) was utilized, where proteins with polyhistidine affinity tags were attracted to cobalt ions on the IMAC column matrix and then eluted with imidazole.

Prior to purification, the transformed BL21 cells containing 6xHis-tagged proteins were grown in 100 ml LB with 100 µg/ml kanamycin at 37 °C. As soon as OD600 reached 0.6, the proteins were induced at 16 °C overnight by addition of 0.3 mM IPTG (Biosolve Chemicals). In the morning cells were centrifuged for 10 minutes at 5000 g at 4 °C, the cell pellet was then frozen in liquid nitrogen and stored at -80 °C.

Prior to the purification, cells containing target proteins were thawed on ice and resuspended in 5 ml of lysis buffer with protease inhibitors and 5 mg of lysozyme (Sigma). Then, the cells were lysed at 4 °C for 15 minutes with stirring every 3 minutes. After the lysis, the cell debris and DNA was further broken down during 3 rounds of 20 seconds sonication, with an ice chill between the sessions. Then, lysate was centrifuged at 21000 g for 20 minutes at 4 °C. Meanwhile, the column with 100 µl Chelating Sepharose (GE Healthcare), was washed with 1 ml of H_2O. Then, 100 µl of 200 mM $CoCl_2$ was added to the matrix and the column was washed with 1 ml of lysis buffer. Following centrifugation, the supernatant was loaded on the column and let to flow through. Subsequently, the unspecific binding of untagged proteins was first washed with Buffer B, and remaining nonspecific proteins were more efficiently eliminated with Buffer C. In the final step target proteins were eluted in 3 aliquots with 100 µl elution buffer each. Second and third aliquots were collected, frozen in liquid nitrogen and stored at -80 °C. After purification, samples were analyzed using SDS-PAGE to estimate purity and concentration of the sample using BSA standards.

3.1.6 Kinase assay

Kinase assay with γ-32P ATP was performed to measure the phosphorylation rate of substrates by Clb5-CDK1. Clb5-CDK1 complexes used in the experiments were purified from *S. cerevisiae* by Rainis Venta as described previously (Kõivomägi et al., 2011).

To achieve equal substrate protein concentrations of 1 µM, substrates were diluted to equal concentration with the elution buffer, 4 µl of the diluted substrate was mixed with 4 µl 50 mM Hepes-KOH (pH 7.4) and kept on ice. Afterward, 0.2 µl of [γ-32P] ATP was added to an enzyme mixture that contained 4 µl of 5xKB, 0.2 µl of BSA, 0.25 µl of purified Cks1 (500 nM final concentration) and 0.2 µl Clb5-CDK1 (0.4 nM final concentration).

Once the mixtures were prepared, the phosphorylation reaction was initiated at room temperature by the addition of 12 µl of enzyme mixture to 8 µl of substrate mixture. The kinase reactions occurred at the initial rate and were terminated at 8 and 16 time points by adding 8 µl of the reaction mix to a tube with 9 µl of SDS loading buffer. Then, the reactions were heated at 72 °C for 5 minutes and subjected to SDS-PAGE. The detection of the transferred γ-32P to the substrates was performed using autoradiography (Typhoon 5 Biomolecular Imager, GE Healthcare Life Sciences), the signals were quantified with the ImageQuant TL (Amersham Biosciences) program.

3.2 RESULTS AND DISCUSSION:

To study the phosphorylation of Far1 N terminus during the cell cycle, time-lapse fluorescence microscopy was used, where Cdk1-dependent phosphorylation of a diphosphodegron can be precisely measured. For this, Far1 N terminus (positions 1-150) was tagged N-terminally with SV40 nuclear localization signal and fused C-terminally with GFP. Far1(1-150)-GFP was expressed under *SIC1* promoter, which is activated in G1 phase as *FAR1* promoter, but gives sufficient expression level also in the absence of pheromone pathway activity. GFP signals were continuously measured in a live-cell fluorescent microscopy experiment, thus the changes in GFP levels quantitatively respond to the changes in Far1(1-150) expression. Also, as the ubiquitin-mediated proteolysis following degron phosphorylation is very rapid, the limiting step in Far1(1-150)-GFP degradation is phosphorylation (Kõivomägi et al., 2011). At the same time our system utilized mCherry fluorescent protein fused to the Whi5 transcriptional repressor that inhibits Start of the cell cycle in late G1. When phosphorylated by CDK1, Whi5 is exported from the nucleus. Therefore, the Start point is defined as Whi5 nuclear levels dropping to 50% of the level in G1 (Doncic et al., 2011). In the analysis of microscopy experiments, different cells are synchronized by the Start point and Far1-GFP levels are followed for 90 minutes after Start, covering the time of an average cell cycle.

3.2.1 NLxxxL is a novel Clb5 docking motif

It was previously shown that the 130-138 region of Far1 could function as a Clb5-specific linear docking motif (manuscript in the attachment). To gain a better understanding of the interaction between Far1 and S-cyclin-CDK1 complex, we introduced several point mutations in the 130-141 region (**Figure 6. a**). As L135 substitution with alanine was previously found to cause a significant delay in degradation, and hydrophobic residues have been found to be of major importance in known cyclin-substrate docking motifs (LP, RxL, LxF), we first wanted to see how single substitutions of other leucines in the putative cyclin docking motif to an amino acid with a smaller side chain, alanine, affect the interaction between Clb5 and Far1.

Whilst the mutant with substituted leucine to alanine in position 136 (L136A) showed no significant difference in Far1 degradation rate compared to WT, the L131A mutation caused a considerable delay of around 40 minutes, similar to L135A (**Figure 6. b, c**). Next, we mutated the asparagine located at position 130 (N130A) and this also led to a 22 minute delay in degradation, although the effect was not as extensive as with L131A and L135A mutations. To test whether the C-terminal flanking region of ^{130}NLTTSLL, ^{137}RESI also contributes to Far1(1-150) phosphorylation, we introduced 4 simultaneous alanine mutations of the RESI sequence (**Figure 6. b, c**). The obtained result shows that there is no difference between RESI mutant and WT, implying that these residues are not essential for efficient Far1 phosphorylation.

The time-lapse microscopy experiments provide means to measure phosphorylation-dependent degradation in the context of the cell cycle. However, as it is an indirect measurement of phosphorylation, we carried out *in vitro* phosphorylation experiments to verify that the detected effects are caused by changes in Clb5-Cdk1-mediated phosphorylation. The performed kinase assays allowed us to track the relative phosphorylation rate of different Far1 mutants by purified Clb5-CDK1 complexes. In this assay a transfer of radioactive phosphate [γ-32P] from ATP to substrates was visualized and quantified by autoradiography. At 8 minutes time point the amount of phosphorylated L131A and L135A mutant was 45 and 48 times lower than WT respectively (**Figure 6. d**). The phosphorylation rate of N130A was 21 times lower compared to WT, consistent with the in vivo experiment, where the N130A mutation caused a significant delay in degradation, but the effect was not as extensive as for L131A and L135A (**Figure 6. d)**. As expected, L136A was rapidly phosphorylated, with almost the same rate as WT. Overall, the four mutants exhibited similar effects both *in vivo* and *in vitro*, indicating that the docking motif contains three key residues that constitute a Clb5-Cdk1 docking motif. Based on the single point substitutions analysed in this work and in the attached manuscript, we postulated that Far1 has a short linear interaction motif (SLiM) [NLxxxL], where asparagine and leucine are followed by three variable amino acids and flanked by another leucine in the C-terminal region.

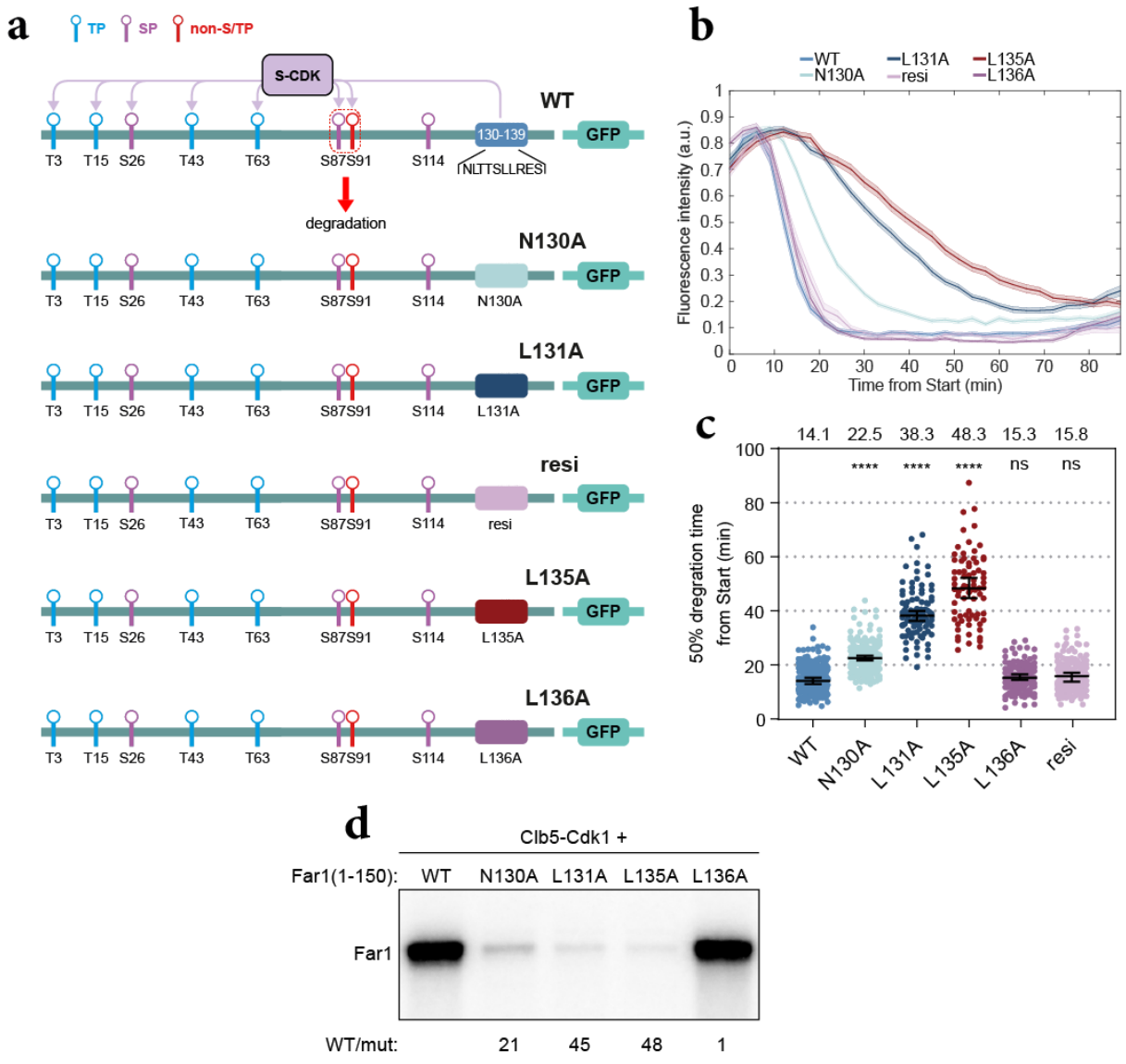

Figure 6. ***In vivo*** **and** ***in vitro*** **mapping of Far1(1-150) docking motif. (a)** The diagram shows several Far1(1-150) docking mutants. Each construct had eight CDK phosphorylation sites, either TP, SP, or the non-proline site S91, two of which (S87 and S91) are essential for Far1 (1-150) degradation. In order to map Clb5-specific docking motif, several alanine substitutions were introduced to 130-139 region of Far1. **(b)** The plot displays degradation dynamics of Far1(1-150)-GFP mutants tracked in fluorescent microscopy experiments. The lines on the graph represent mean±SEM of Far1(1-150) GFP fluorescence intensities. The start point (0) is denoted as 50% of Whi5 export from the nucleus. **(c)** The analysis of Far1(1-150)-GFP degradation in single cells. The values displayed at the top of the graph report the median time for mutant cells to experience a 50% decrease in protein concentration. (d) Autoradiograph from kinase assay that shows Far1 docking mutants specificity towards Clb5-CDK1.

Together the presented *in vivo* and *in vitro* results confirm that NLxxxL is a novel SLiM that enhances Far1 phosphorylation by Clb5-CDK1. This docking motif does not directly resemble the known S-phase RxL docking motif with a consensus R/K-x-L-φ. However, as many previously discovered cyclin docking motifs, NLxxxL has three esential residues that define the motif, while other flanking positions have minor effects. NLxxxL motif was found to be exclusively specific for Clb5-Cdk1, and not Clb3- or Clb2-Cdk1 (manuscript in supplementary). The novel Clb5 specific docking motif could also explain the functional difference between Clb5 and Clb6, that to the date is not completely understood. At this point, however, it is not known whether NLxxxL promotes phosphorylation by Clb6-Cdk1.

3.2.2 NLxxxL motif functions in Lif1

Next, having mapped the Clb5 docking motif in Far1, we screened the yeast proteome, limiting the search to the intrinsically disordered regions, to identify additional substrates whose phosphorylation could be regulated by this SLiM. The results showed 127 proteins contained potential NLxxxL docking motifs and 50 of them were targeted by CDK1. It has been demonstrated previously that at least 4 proteins from the search (Lif1, Fin1, Yen1, Sld3) have been found to interact with Clb5 and several others, such as Fin1 and Spc110 are known Clb5-Cdk1 targets (**Figure 7. a**). Lif1, for example, is a component of DNA ligase IV complexes in yeast that rejoins DNA double-strand breaks (DSBs) by non-homologous end joining. It was previously shown that this substrate is targeted by the Clb5-CDK1 complex during S phase, however, the mechanism of substrate-cyclin interaction was unknown (reference). To identify the Clb5 cyclin specificity towards Lif1, we performed an *in vitro* kinase assay with two constructs: wild type Lif1 (WT) and Lif1 lacking the NLxxxL motif (nlxxxl). The obtained autoradiograph (**Figure 7. b**) indicates that the NLxxxL motif, located in the C-terminal side at an optimal distance from a CDK1 consensus site (S264), is required for efficient Lif1 phosphorylation by Clb5-Cdk1.

From the outcome of the NLxxxL motif prediction and verification of the motif in Lif1 it can be concluded that NLxxxL docking motif is functional in other Clb5-Cdk1 targets. Therefore,

the NLxxxL motif could contribute to timely phosphorylation of a wider range of S phase Cdk1 targets.

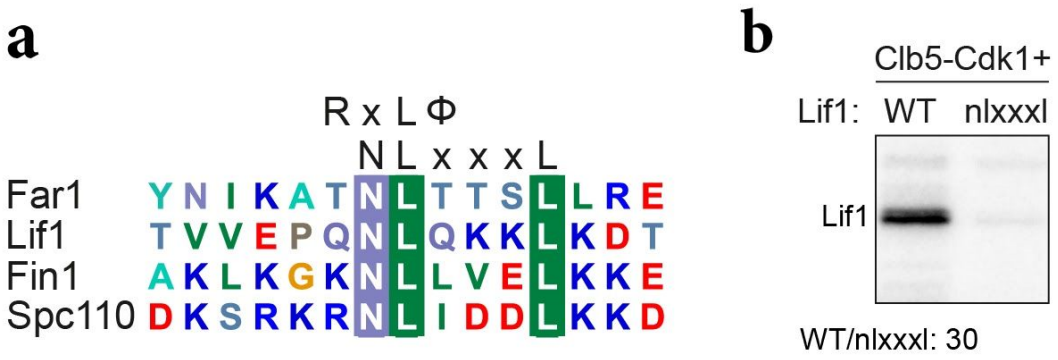

Figure 7. ***In vitro*** **analysis of NLxxxL functionality in Lif1. (a)** An alignment of substrates with potential NLxxxL docking motif. **(b)** Autoradiograph from kinase assay that shows Lif1 specificity towards Clb5-CDK1. The WT/nlxxxl is the ratio of Lif1 phosphorylation efficiency with and without NLxxxL docking motif.

3.2.3 Homology of NLxxxL and RxL motifs

K/R-x-L-φ is a classical cyclin docking motif found in a wide variety of S-phase cyclin-CDK1 targets. Fin1, for instance, a protein that associates with and stabilizes microtubules during anaphase, contains ^{194}KxL^{196} docking motif that tightly binds the hydrophobic patch of Clb5-CDK1 complex. While screening for potential NLxxxL motifs in yeast, we found that ^{194}**KNL**LVE**L**^{200} sequence in Fin1 has an overlap of potential NLxxxL motif and the previously characterized RxL motif. Furthermore, alignments of S-phase targets with identified RxL docking motifs in yeasts revealed that RxL docking sequences in several substrates overlap with NLxxxL docking motif determinants (manuscript in supplementary). This suggests that the two motifs, RxL and NLxxxL, could potentially evolve from the same origin.

To investigate the potential overlap of the two motifs further, RxL determinants were introduced to Far1(1-150)-GFP to study if this improves phosphorylation specificity. To gain better resolution of constructs with different docking sites, all threonine phosphosites (TP) in Far1(1-150) were mutated to serine phospho residues (SP), as an adaptor subunit Cks1 binds

only phospho-threonines, this way Cks1-mediated increase in phosphorylation efficiency is eliminated and phosphorylation could be more dependent on cyclin docking (**Figure 8. a**). Following inactivation of Cks1 priming site, we created several overlapping versions of NLxxxL and RxL docking motifs in Far1(1-150) mutant. Introduction of the RxL determinants, the **KNL**TTS**L** (SP T129K) and **RNLF**TSL (SP RNLF), however, did not significantly alter Far1(1-150 SP)-GFP degradation, indicating that these residues do not enhance the interaction with Clb5 (**Figure 8. b, c**). On the other hand, amino acids introduced from conventional RxL docking motif, caused drastical delays in degradation of 40 and 60 minutes in PRKLQF (SP PRKLQF) and PKKLQF (SP PKKLQF) respectively, suggesting that NLxxxL motif has a higher binding affinity towards Clb5-CDK1 complex than RxL.

Moreover, previous studies revealed that Far1(1-150) with NLxxxL docking motif reaches half of the maximum phosphorylation rate (½Vmax) at lower concentration of substrates than Far1(1-150) with RxL (manuscript in supplementary). These results support our hypothesis that substrates with NLxxxL docking motif exhibit higher specificity towards the Clb5-Cdk1 complex than RxL. Furthermore, the experiment shows that different RxL motifs also lead to different timing of phosphorylation, suggesting that cyclin docking motif affinity could contribute significantly to the ordering of the Cdk1-dependent phosphorylation events in the cell cycle.

Based on the alignments of S phase targets above we can also speculate that the NLxxxL and the RxL docking motif, that is present in many S phase substrates, could evolve from common ancestor. During pheromone signalling Far1 tightly binds Clb5-CDK1 complex and inhibits cell cycle progression. The stronger binding affinity of NLxxxL towards Clb5 could suggest a mechanism of how Far1 displaces other S phase substrates with weaker cyclin-specific docking motifs during cell cycle arrest.

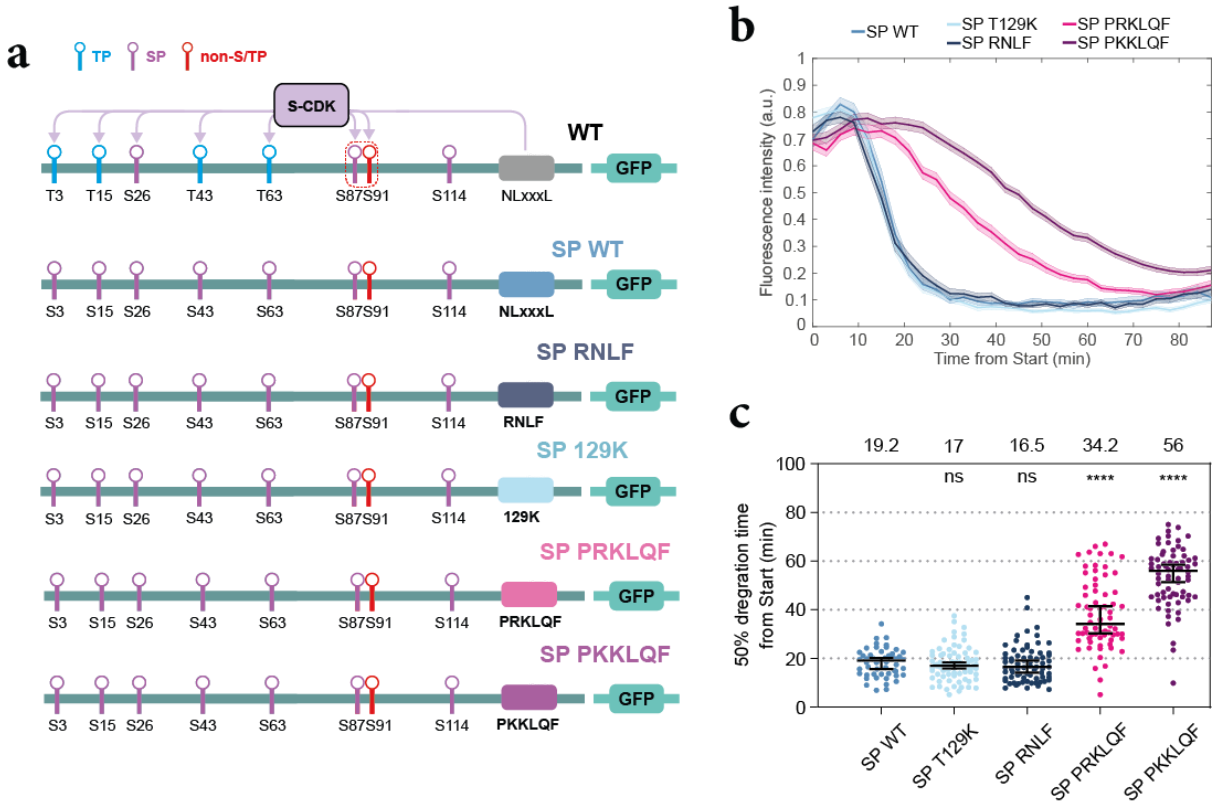

Figure 8. RxL determinants integrated in NLxxL docking motif. **(a)** The diagram shows Far1 (1-150) constructs where all threonine phosphosites (TP) were swapped to serines (SP). At the same time, RxL docking motif determinants were introduced in NLxxxL docking sequence to study homology of these two docking motifs. **(b)** The plot shows degradation dynamics of Far1(1-150) SP docking mutants tracked in fluorescent microscopy experiments. The lines on the graph represent mean±SEM of Far1(1-150) GFP fluorescence intensities. The start point (0) is denoted as 50% of Whi5 export from the nucleus. **(c)** The analysis of Far1(1-150)-GFP sensors degradation in single cells. The values displayed at the top of the graph report the median time for mutant cells to experience a 50% decrease in protein concentration.

3.2.4 The contribution of Cks1 to the degron phosphorylation depends on the cyclin docking motif.

When the Cks1 phosphoadaptor subunit of cyclin-CDK1-Cks1 complex binds a priming site on a substrate, it promotes N-to-C terminal sequential phosphorylation of other residues by CDK1. To test how Cks1 contributes to the phosphorylation efficiency in the context of different docking motifs, the length of Far1 was limited to positions 85-150 (**Figure 9. a**). The Far1 (85-150) segment still had one CDK1 consensus site in addition to the degron

essential for its degradation, but the other four phosphosites and Cks1 priming site (T3) in the N terminus were missing. Having only one primer site, Far1(85-150) represented a minimal model for studying the Cks1 multisite potentiation effect. After elimination of Cks1 binding sites, we constructed several Far1(85-150) mutants with variable docking motifs: NLxxxL (WT), RxL and a mutated docking motif, where three leucines at positions 131, 135 and 136 were substituted with alanines (nlxxxl). As the next step, T3 priming site was added to each of the constructs resulting in three additional constructs with priming site (**Figure 9. a**).

The obtained results showed that NLxxxL substitution in Far1(85-150) with RxL increased the degradation time to about 60 minutes (**Figure 9. b, c**). This data supports the previous findings that NLxxxL docking motif posesses higher binding affinity towards the Clb5-CDK1 complex than RxL. As expected, the nlxxxl mutant led to a drastic delay in Far1(85-150) degradation, but when enhanced by distal Cks1 interactions, nlxxxl+T3 was degraded more rapidly. Interestingly, when associated with Cks1 priming site, the RxL+T3 mutant was degraded almost three times faster than the RxL construct (**Figure 9. b, c**). In line with previous studies this suggests that substrates with RxL docking motif require Cks1 subunit for efficient phosphorylation. On the other hand, NLxxxL mutant in the absence of the Cks1 priming site showed similar degradation behaviour as NLxxxL+T3, as the Far1(85-150) protein concentration in the cells was halved at around 16 minutes for both constructs. This data is consistent with our previous findings, indicating that NLxxxL alone could be sufficient for efficient Far1 multisite phosphorylation (manuscript in supplementary).

These results suggest a mechanism of how distal docking interactions could enhance the otherwise weak cyclin binding affinities in substrates. Research showed that the weak specificity of RxL docking motif towards Clb5 is strengthened by Cks1 binding sites. Efficient phosphorylation of substrates with weak docking interactions reveals the importance of interactions that occur outside of the CDK1 catalytic domain. These interactions can stimulate precise ordering of cell cycle events by CDK1.

Another interesting discovery was the ability of NLxxxL docking motif to independently promote efficient protein phosphorylation in the absence of Cks1-directed phosphorylation. This suggests that the Cks1 interaction networks have smaller importance in case of highly

specific docking motifs.

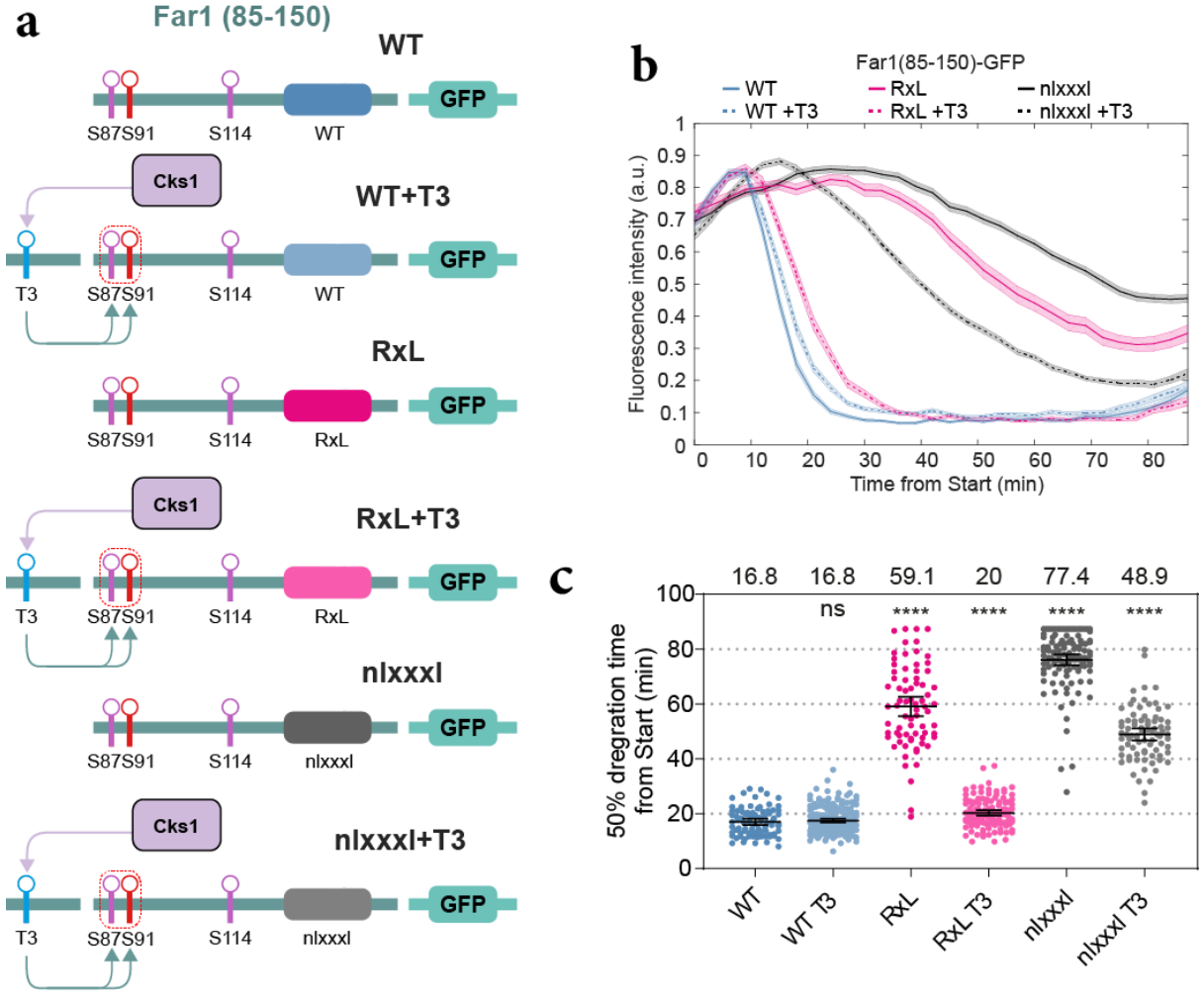

Figure 9. The context of docking motifs in Cks1-mediated phosphorylation. (a) The diagram shows Far1(85-150) constructs with three docking motif variations. In addition, each docking motif was tested in the presence and absence of Cks1 priming site (T3) forming six Far1(85-150) mutants. **(b)** The plot displays degradation dynamics of Far1(85-150)-GFP sensors tracked in fluorescent microscopy experiments. The lines on the graph represent mean±SEM of Far1(85-150) GFP fluorescence intensities. The start point (0) is denoted as 50% of Whi5 export from the nucleus. **(c)** The analysis of Far1(85-150)-GFP degradation in single cells. The values displayed at the top of the graph report the median time for mutant cells to experience a 50% decrease in protein concentration.

4 SUMMARY

Cyclin-CDK complexes initiate various cell cycle events by phosphorylating different sets of proteins. The temporal order of the cell cycle events is dependent on cyclins that bind to docking motifs in substrates and enhance phosphorylation of specific proteins by the kinase.

The results presented in this study cast a new light on substrate targeting by cyclin-CDK1 complexes. A novel Clb5-specific docking motif present in CDK1 inhibitory protein Far1 was identified using site-directed mutagenesis. This study revealed that single point mutations in positions 130, 131 and 135 of Far1(1-150) significantly altered its phosphorylation dynamics in the cell cycle. Other mutations of the 130-140 region in Far1 showed no significant difference in degron phosphorylation indicating that only three residues are essential in Far1-Clb5 docking interactions, indicating that this takes place via a novel short linear motif NLxxxL.

Further analysis showed that NLxxxL is functional in other Clb5-Cdk1 targets and therefore may contribute to a higher degree of S-phase-specific substrate phosphorylation. Moreover, an alignment of several substrates that were previously thought to bind S-phase cyclins via RxL docking motif showed conservation of NLxxxL determinants in their RxL docking region, suggesting that two motifs could arise from a common ancestor. A comparative analysis of known S-phase docking motif RxL and a novel Clb5-specific SLiM NLxxxL revealed that the latter exhibits higher binding specificity towards Clb5. Stronger binding affinity of NLxxxL docking motif could explain the mechanism of how Far1 inhibitory protein outcompetes S-phase substrates containing RxL docking sequence for binding with Clb5-CDK1 complex during the cell cycle arrest.

Another interesting finding emerged from studying Cks1-dependent phosphorylation of substrates containing RxL and NLxxxL docking motifs. The results showed that Cks1 aids in phosphorylation of CDK targets with otherwise weak docking motifs, whereas high affinity docking peptide NLxxxL can independently promote multisite phosphorylation of S-phase substrates. The understanding of the cell cycle is essential when trying to tackle serious diseases and design therapeutics.

References

Basu S, Roberts EL, Jones AW, Swaffer MP, Snijders AP, Nurse P. (2020). The Hydrophobic Patch Directs Cyclin B to Centrosomes to Promote Global CDK Phosphorylation at Mitosis. Curr Biol. 30(5):883‑892.e4.

Bavle R. M. (2014). Mitosis at a glance. Journal of oral and maxillofacial pathology : JOMFP, 18(Suppl 1), S2–S5.

Bhaduri, S., and Pryciak, P.M. (2011). Cyclin-Specific Docking Motifs Promote Phosphorylation of Yeast Signaling Proteins by G1/S Cdk Complexes. Curr. Biol. 21, 1615–1623.

Bloom, J., & Cross, F. R. (2007). Multiple levels of cyclin specificity in cell-cycle control. *Nature reviews. Molecular cell biology*, *8*(2), 149–160.

Chang, F., & Herskowitz, I. (1990). Identification of a gene necessary for cell cycle arrest by a negative growth factor of yeast: FAR1 is an inhibitor of a G1 cyclin, CLN2. *Cell*, *63*(5), 999–1011.

Cooper, G.M.(2000). The Cell: A Molecular Approach. 2nd edition.(The Eukaryotic Cell Cycle).

Coudreuse, D., & Nurse, P. (2010). Driving the cell cycle with a minimal CDK control network. *Nature*, *468*(7327), 1074–1079.

Cross, F. R., Archambault, V., Miller, M., & Klovstad, M. (2002). Testing a mathematical model of the yeast cell cycle. *Molecular biology of the cell*, *13*(1), 52–70.

Cross, F. R., Buchler, N. E., & Skotheim, J. M. (2011). Evolution of networks and sequences in eukaryotic cell cycle control. *Philosophical transactions of the Royal Society of London. Series B, Biological sciences*, *366*(1584), 3532–3544.

Donaldson, A. D., Raghuraman, M. K., Friedman, K. L., Cross, F. R., Brewer, B. J., & Fangman, W. L. (1998). CLB5-dependent activation of late replication origins in S. cerevisiae. *Molecular cell*, *2*(2), 173–182.

Doncic, A., Atay, O., Valk, E., Grande, A., Bush, A., Vasen, G., Colman-Lerner, A., Loog, M., & Skotheim, J. M. (2015). Compartmentalization of a bistable switch enables memory to cross a feedback-driven transition. *Cell*, *160*(6), 1182–1195.

Enserink, J. M., & Kolodner, R. D. (2010). An overview of Cdk1-controlled targets and processes. *Cell division*, *5*, 11.

Fitch, I., Dahmann, C., Surana, U., Amon, A., Nasmyth, K., Goetsch, L., Byers, B., & Futcher, B. (1992). Characterization of four B-type cyclin genes of the budding yeast Saccharomyces cerevisiae. *Molecular biology of the cell*, *3*(7), 805–818.

Fragkos M, Ganier O, Coulombe P, Méchali M. (2015). DNA replication origin activation in space and time. Nat Rev Mol Cell Biol. 16(6):360‑374.

Gérard, C., Tyson, J. J., Coudreuse, D., & Novák, B. (2015). Cell cycle control by a minimal Cdk network. *PLoS computational biology*, *11*(2), e1004056.

Holt, L.J., Tuch, B.B., Villen, J, Johnson, A.D., Gygi, S.P., Morgan, D.O. (2009). Global analysis of Cdk1 substrate phosphorylation sites provides insights into evolution. Science 325, 1682–1686

Hu, F., & Aparicio, O. M. (2005). Swe1 regulation and transcriptional control restrict the activity of mitotic cyclins toward replication proteins in Saccharomyces cerevisiae. *Proceedings of the National Academy of Sciences of the United States of America*, *102*(25), 8910–8915.

Huang, D., Friesen, H., Andrews, Brenda. (2007). PHO85, a multifunctional cyclin-dependent protein kinase in budding yeast. Molecular microbiology. 66. 303-14.

Jackson, L. P., Reed, S. I., & Haase, S. B. (2006). Distinct mechanisms control the stability of the related S-phase cyclins Clb5 and Clb6. *Molecular and cellular biology*, *26*(6), 2456–2466.

Jeffrey, P. D., Russo, A. A., Polyak, K., Gibbs, E., Hurwitz, J., Massagué, J., & Pavletich, N. P. (1995). Mechanism of CDK activation revealed by the structure of a cyclinA-CDK2 complex. *Nature*, *376*(6538), 313–320.

Kaldis P, Sutton A, Solomon MJ. The Cdk-activating kinase (CAK) from budding yeast. *Cell*. 1996;86(4):553‑564. doi:10.1016/s0092-8674(00)80129-4

Kõivomägi, M., Örd, M., Iofik, A., Valk, E., Venta, R., and Faustova, I. (2013). Multisite phosphorylation networks as signal processors for Cdk1. Nat Struct Mol Biol. 20, 1–24.

Kõivomägi, M., Valk, E., Venta, R., Iofik, A., Lepiku, M., Balog, E. R., Rubin, S. M., Morgan, D. O., & Loog, M. (2011). Cascades of multisite phosphorylation control Sic1 destruction at the onset of S phase. *Nature*, *480*(7375), 128–131.

Kõivomägi, M., Valk, E., Venta, R., Iofik, A., Lepiku, M., Morgan, D.O., and Loog, M. (2011). Dynamics of Cdk1 Substrate Specificity during the Cell Cycle. Mol. Cell 42, 610–623.

Lim, W., Mayer, B., & Pawson, T. (2015). *Cell signaling: Principles and mechanisms*.

Lindon C. (2008). Control of mitotic exit and cytokinesis by the APC/C. *Biochemical Society transactions*, *36*(Pt 3), 405–410.

Lu, D., Hsiao, J. Y., Davey, N. E., Van Voorhis, V. A., Foster, S. A., Tang, C., & Morgan, D. O. (2014). Multiple mechanisms determine the order of APC/C substrate degradation in mitosis. *The Journal of cell biology*, *207*(1), 23–39.

Malumbres, M., Barbacid, M. Mammalian cyclin-dependent kinases. *Trends Biochem Sci*. 2005;30(11):630‑641.

McGrath, D. A., Balog, E. R., Kõivomägi, M., Lucena, R., Mai, M. V., Hirschi, A., Kellogg, D. R., Loog, M., & Rubin, S. M. (2013). Cks confers specificity to phosphorylation-dependent CDK signaling pathways. *Nature structural & molecular biology*, *20*(12), 1407–1414.

Mendenhall, M.D., Hodge, A. E.(1998). Microbiology and Molecular Biology Reviews, 62 (4) 1191-1243;

Morgan D. O. (1997). Cyclin-dependent kinases: engines, clocks, and microprocessors. *Annual review of cell and developmental biology*, *13*, 261–291.

Morgan, D.O. (2007). The Cell Cycle: Principles of Control (London: New Science Press Ltd).

Ondracka, A., Robbins, J. A., & Cross, F. R. (2016). An APC/C-Cdh1 Biosensor Reveals the Dynamics of Cdh1 Inactivation at the G1/S Transition. *PloS one*, *11*(7), e0159166.

Örd, M., & Loog, M. (2019). How the cell cycle clock ticks. *Molecular biology of the cell*, *30*(2), 169–172.

Örd, M., Venta, R., Möll, K., Valk, E., & Loog, M. (2019). Cyclin-Specific Docking Mechanisms Reveal the Complexity of M-CDK Function in the Cell Cycle. *Molecular cell*, *75*(1), 76–89.e3.

Patra, D., & Dunphy, W. G. (1998). Xe-p9, a Xenopus Suc1/Cks protein, is essential for the Cdc2-dependent phosphorylation of the anaphase- promoting complex at mitosis. *Genes & development*, *12*(16), 2549–2559.

Patra, D., Wang, S. X., Kumagai, A., & Dunphy, W. G. (1999). The xenopus Suc1/Cks protein promotes the phosphorylation of G(2)/M regulators. *The Journal of biological chemistry*, *274*(52), 36839–36842.

Peter, M., Gartner, A., Horecka, J., Ammerer, G., & Herskowitz, I. (1993). FAR1 links the signal transduction pathway to the cell cycle machinery in yeast. *Cell*, *73*(4), 747–760.

Pines, J. (1996). Cell cycle: Reaching for a role for the Cks proteins. *Current Biology, 6*, 1399-1402.

Pope, P.A., Bhaduri, S., and Pryciak, P.M. (2014). Regulation of Cyclin-Substrate Docking by a G1 Arrest Signaling Pathway and the Cdk Inhibitor Far1. Curr. Biol. 24, 1390–1396.

Rahal, R., & Amon, A. (2008). Mitotic CDKs control the metaphase-anaphase transition and trigger spindle elongation. *Genes & development*, *22*(11), 1534–1548.

Richardson, H.E., Wittenberg, C., Cross, F., and Reed, S.I. (1989). An essential G1 function for cyclin-like proteins in yeast. Cell 59, 1127–1133.

Ross, K. E., Kaldis, P., & Solomon, M. J. (2000). Activating phosphorylation of the Saccharomyces cerevisiae cyclin-dependent kinase, cdc28p, precedes cyclin binding. *Molecular biology of the cell*, *11*(5), 1597–1609.

Schwob, E., & Nasmyth, K. (1993). CLB5 and CLB6, a new pair of B cyclins involved in DNA replication in Saccharomyces cerevisiae. *Genes & development*, *7*(7A), 1160–1175.

Shi, L., & Tu, B. P. (2013). Acetyl-CoA induces transcription of the key G1 cyclin CLN3 to promote entry into the cell division cycle in Saccharomyces cerevisiae. *Proceedings of the National Academy of Sciences of the United States of America*, *110*(18), 7318–7323.

Swaffer, M. P., Jones, A. W., Flynn, H. R., Snijders, A. P., & Nurse, P. (2016). CDK Substrate Phosphorylation and Ordering the Cell Cycle. *Cell*, *167*(7), 1750–1761.

Tyanova, S., Cox, J., Olsen, J., Mann, M., Frishman, D. (2013). Phosphorylation variation during the cell cycle scales with structural propensities of proteins. PLoS Comput Biol 9, e1002842.

Tyers, M., Tokiwa, G., & Futcher, B. (1993). Comparison of the Saccharomyces cerevisiae G1 cyclins: Cln3 may be an upstream activator of Cln1, Cln2 and other cyclins. *The EMBO journal*, *12*(5), 1955–1968.

Vogt, P.K., Reed, S.I. (1998). Cyclin Dependent Kinase (CDK) Inhibitors.

Wilmes, G. M., Archambault, V., Austin, R. J., Jacobson, M. D., Bell, S. P., & Cross, F. R. (2004). Interaction of the S-phase cyclin Clb5 with an "RXL" docking sequence in the initiator protein Orc6 provides an origin-localized replication control switch. *Genes & development*, *18*(9), 981–991.

Wittenberg, C., Sugimoto, K., & Reed, S. I. (1990). G1-specific cyclins of S. cerevisiae: cell cycle periodicity, regulation by mating pheromone, and association with the p34CDC28 protein kinase. *Cell*, *62*(2), 225–237.

Yang, Q., & Ferrell, J. E., Jr (2013). The Cdk1-APC/C cell cycle oscillator circuit functions as a time-delayed, ultrasensitive switch. *Nature cell biology*, *15*(5), 519–525.

Yang, X., Lau, K. Y., Sevim, V., & Tang, C. (2013). Design principles of the yeast G1/S switch. *PLoS biology*, *11*(10), e1001673.

APPENDIX

Exclusively S-CDK-specific signaling via docking of a linear motif

Ilona Faustova, Luka Bulatovic, Frida Matiyevskaya, Ervin Valk, Mihkel Örd, and Mart Loog

Institute of Technology, University of Tartu, Tartu, 50411, Estonia

Abstract

Cyclin-dependent kinases (CDKs), the master regulators of cell division, are activated by different cyclins at different cell cycle stages. In addition to being activators of CDKs, cyclins have been found to accommodate various linear motifs in substrates, targeting CDK activity to specific proteins. To control the cell cycle, *S. cerevisiae* Cdk1 phosphorylates up to 500 proteins in a timely resolved manner. By studying the multisite phosphorylation of CDK substrate and inhibitor protein Far1, we uncovered a novel S-phase cyclin docking motif that mediates Far1 phosphorylation-dependent degradation at G1/S. We show that the discovered motif is highly specific for S-CDK and can function as a modular docking motif. Using time-lapse fluorescence microscopy, we show how different docking connections control timely phosphorylation of Far1 di-phosphodegron. We found the discovered Far1 docking motif to be more efficient in targeting S-CDK activity compared to the conventional RxL motif found in many S-phase CDK targets. The high affinity cyclin docking motif is able to promote direct phosphorylation of the di-phosphodegron, while in case of lower affinity RxL docking, a secondary docking via Cks1 is also necessary. Our results show how the balance between the docking via priming phosphorylation and docking via cyclin-binding motifs can control the timing of CDK controlled switching.

Introduction

Cyclin-dependent protein kinases (CDKs) are central regulators executing hundreds of phosphorylation events that trigger, order, check, and finalize the complex process of eukaryotic cell division cycle (Enserink and Kolodner, 2010; Morgan, 2007). CDKs are unique among hundreds of other representatives of the eukaryotic protein kinase superfamily, as they use complex sequential multi-docking phosphorylation mechanisms that involve interactions with combinations of short linear motifs (SLiMs) in their target proteins (Örd and Loog, 2019).

Initial view of cyclins, as periodically synthesized and degraded activating proteins of CDK kinase complex, each acting at their specific cell cycle stage, has been considerably broadened recently. First, it was found that cyclins are not merely activating subunits of CDK, but different cyclins also introduce a possibility to modulate the intrinsic active-site specificity towards the phosphorylation motifs. This finding, first discovered for yeast Cdk1 complexes and a histone-based short peptide substrate (Kõivomägi et al., 2011a; Loog and Morgan, 2005), is now corroborated also with human CDK complexes (Topacio et al., 2019). Secondly, for a long time it was known that a subset of CDK targets are tethered to CDK complexes via specific RXL docking motifs (a SLiM with the consensus sequence R/K-x-L-ϕ or R/K-x-L-x $-\phi$) that bind to a hydrophobic pocket, called hydrophobic patch (*hp*) in human cyclin A or E (Russo et al., 1996; Schulman et al., 1998; Takeda et al., 2001) or in S-phase cyclin Clb5 in budding yeast (Loog and Morgan, 2005; Wilmes et al., 2004). However, recent studies have uncovered several other cyclin-specific SLiMs that interact either with the *hp* or other areas on the cyclins (Bhaduri and Pryciak, 2011; Bhaduri et al., 2015; Kõivomägi et al., 2011a; Örd et al., 2019a; Topacio et al., 2019). These studies widened the scope of the third general function of cyclins: in addition to being an activator and activity modulating factor for Cdk subunit, cyclins also act as protein scaffolds presenting various pockets to dock different SLiMs in target proteins. The full set of highly specific and selective motifs for the four major cyclins in budding yeast: the LP, RXL, PXF, and LXF motifs for G1-, S-, G2-, and M-phase cyclins, respectively,

have been defined recently (Bhaduri and Pryciak, 2011; Kõivomägi et al., 2011a; Örd et al., 2019a) that altogether define cyclins as proteins presenting a plethora of docking options for SLiMs to achieve specific cell cycle signaling via CDK phosphorylation.

Such a complexity of substrate docking motifs begins to highlight the uniqueness of CDK among other protein kinases. Its grandiose task to temporally order hundreds, if not thousands, of individual phosphorylation events during the cell cycle is quite different compared to the task assigned to many other kinases and signaling enzymes, whose action mode can be described as binary switching between active and inactive state. In addition to the differential docking mechanisms provided by cyclins, the key to the combinatorial complexity of CDK substrate phosphorylation is based on Cks1, a phospho-adaptor subunit (Kõivomägi et al., 2011b; McGrath et al., 2013), an entirely unique feature of CDK complex among protein kinases. The majority of CDK targets contain multiple phosphorylation sites in intrinsically disordered regions (Holt et al., 2009), and the cyclin-Cdk1-Cks1 complex functions as a scaffold with three fixed docking points (**Fig. 1A**), to process the multi-site phosphorylation in an ordered manner (Kõivomägi et al., 2013; Örd et al., 2019b). The phosphorylated TP motifs bind to the Cks1 phospho-pocket and facilitate the phosphorylation of secondary sites located C-terminally from the pTP priming sites (Kõivomägi et al., 2013; McGrath et al., 2013). Such mechanism enables phosphorylated Cks1-binding motifs, CDK active site binding phosphorylation motifs, and diverse cyclin binding motifs to be combined in a sort of “barcoded” linear patterns along the disordered targets. These patterns can be read by the CDK complexes to achieve different input-output function of the net phosphorylation rate for a target (Örd et al., 2019b). With other words, the barcoded patterns act as timing tags that assign a target to a specific CDK activity threshold, and thereby, designate its role to be executed at specific time-point during the cell cycle.

The SLiM motifs positioned in linear combinations along the disordered segments of CDK targets have individual affinities and/or K_M values in the range of 10-500 μM (Loog and Morgan, 2005; McGrath et al., 2013; Wohlschlegel et al., 2001). The SLiMs with a range of micromolar affinities, when combined at certain linear patterns can together encode different CDK thresholds that assign the phosphorylation switches to take place at precisely determined time-points along the axis of cell cycle progression (Örd et al., 2019b; Swaffer et al., 2016). On the other hand, the CDK inhibitors based on disordered proteins can achieve net affinities in low nanomolar range by combining larger number of SLiMs or longer binding regions, like demonstrated for p27 in human cells (Russo et al., 1996), and Sic1 and Far1 in budding yeast ((Venta et al., 2020), Valk & Loog, manuscript in preparation). How such a wide affinity range spanning from low nanomolar for inhibitors to micromolar for substrates is achieved by combining the SLiMs is not entirely understood, and so far, there is a lack of knowledge of SLiMs that may have higher affinity than the ones known so far (exemplified above). It is also not clear how the two major elements of multisite substrate docking, the Cks1-binding priming phosphorylation site, located in N-terminal direction from the phosphorylation site, and the cyclin-binding SLiM, located at C-terminal side (**Fig. 1A**), are cooperating or compensating each other’s effects in defining phosphorylation efficiencies, and thus the CDK thresholds and timings of the cell cycle events.

Here we report a SLiM docking motif NLxxxL for a *S. cerevisiae* S-phase cyclin, which stands out among the known cyclin docking sites due to its higher affinity to cyclin. We show how such motif can compensate the absence of Cks1-dependent priming mechanism and how different CDK thresholds can be encoded by combining different cyclin- and Cks1-binding SLiMs into one CDK target with a phosphodegron output signal. Furthermore, the NLxxxL motif promotes exclusively S-CDK-specific phosphorylation of other targets. In addition to controlling the CDK thresholds during the accumulation of cyclins, we show how the cyclin specificity contributes to CDK substrate dephosphorylation in anaphase. By achieving tight control over cell cycle timing of

phosphorylation-dependent destruction of the disordered substrate construct, we demonstrate how such protein segment can be used as a protein timing tag to precisely control its temporal expression profile relatively to cell cycle stages. We will discuss how such ability to precisely control dynamics of protein activities may be useful for different practical applications in biotechnology.

Results

S-CDK-specific cyclin docking motif promotes phosphorylation of phospho-degron in Far1

An S-CDK-specific putative linear docking motif was initially mapped via truncations of the N-terminal disordered region of Far1 within the segment of 130-140 of Far1 (unpublished data). In the current study, the motif was then further mapped using site-directed mutagenesis and quantitative time-lapse fluorescence microscopy. For this, we employed an approach using CDK threshold sensors, a set of variable GFP-tagged substrate constructs that are degraded in response to phosphorylation at defined levels of CDK activity (Örd et al., 2019b). We based the sensors on a fragment composed of the first 150 N-terminal amino acids from Far1 (1-150-Far1) (**Fig. 1B**). This fragment contained a di-phospho-degron (S87&S91), a pair of CDK phosphorylation sites essential for Far1 degradation (Valk & Loog, manuscript in preparation). To analyze the effects of systematic alanine mutations within the docking motif on CDK-dependent phosphorylation of the degron, we measured the dynamics of sensor degradation. Ubiquitination-driven degradation of phosphorylated sensors is mediated by E3 ligase SCF-Cdc4 and proteasome, that are constitutively active throughout the cell cycle (Zhou and Howley, 1998), allowing to measure the dynamics of CDK activity alone. Using a previously described live-cell fluorescent microscopy protocol (Örd et al., 2019b), we followed the timing of phosphorylation-dependent degradation of GFP-tagged sensors (**Fig. 1C, D**). For time-point zero, we used the cell cycle *Start*, defined as the nuclear export of 50% of Whi5-mCherry, the transcriptional inhibitor of early cell cycle genes (Doncic et al., 2011). As for the time-window of the assay, we demonstrated that a construct based on the wild type 1-150-Far1 was degraded rapidly, declining to 50% of its maximal levels by ~13 minutes from *Start* (**Fig. 1D**). This is in good agreement with our previous observations of the timing of G1/S transition, marked by Sic1 degradation and accumulation of free Clb5-Cdk1 complex (Venta et al., 2020). On the other hand, the double-alanine mutant of the di-phosphodegron stabilized the sensor for the length of the cell cycle, which for budding yeast in rich media is about 90 minutes (**Fig. 1C, D**).

We introduced alanine mutations within the identified region and tested a set of them in the context of the CDK threshold sensors (**Fig. 1E, F**). Single mutants L131A, and L135A showed a considerable delay in sensor degradation, the mutation N130A caused an intermediate effect with a ~22-minute half time, while L136A mutation, and a triple mutation of the motif TTS in the middle of the segment behaved like a wild type. We also introduced simultaneous alanine mutants into four amino acid segments flanking the 10 amino acid region initially mapped by truncations. The 4xAla mutations of the N-terminal flanking sequence IKAT and the C-terminal RESI caused no delay in degradation, neither individually nor in combination (**Fig. 1E, F**).

As the sequence of the segment did not bear any obvious resemblance to the conventional RxLxF motif, we wondered if a sequence region between the docking motif and the phosphorylation sites would provide crucial additional contacts with the CDK complex. To test this, we replaced two segments in this linker region with Gly-Ser stretches (**Suppl. Fig. 1A**). However, no differences in degradation dynamics was observed compared to the control sensor (**Suppl. Fig. 1B, C**). These results indicate that the docking specificity is provided by the NLxxxL motif, and such motif fulfills the general criteria of a Short Linear motif (SLiM), generally defined as amino acid consensus motifs covering a disordered segment of up to ten amino acids (Davey et al., 2012).

To compare the *in vivo* data with the biochemical measurements of CDK specificity *in vitro*, we performed assays to determine the initial velocity of phosphorylation using purified CDK complexes and the sensor proteins, and ^{32}P autoradiography of SDS-PAGE. Strikingly, the key mutants N130A, L131A, L135A showed similar relative specificity as the degradation order observed in vivo (**Fig. 1G**). To analyze the cyclin specificity of the identified docking motif, we performed *in vitro* phosphorylation assays with four major cyclin-Cdk1 complexes and their corresponding cyclin docking pocket mutants (**Fig. 1H**). As controls (i) histone H1, a substrate not affected by cyclin docking, and relying only on phosphorylation site consensus motif, and (ii) a non-inhibitory truncated version of Cdk1 inhibitor Sic1 (Sic1ΔC), containing a conventional cyclin docking motif RxLxF, were used. The obtained results clearly show that the discovered docking motif was exclusively specific for S-phase complex Clb5-Cdk1. The other closely related G2- and M-CDK complexes (Clb3- and Clb2-Cdk1) showed very weak phosphorylation rate. The G1-Cdk1 complex Cln2-Cdk1, also showed considerable phosphorylation specificity, however, this was neither dependent on the discovered motif in Far1, nor of the known hydrophobic substrate binding pocket on Cln2 (Bhaduri et al., 2015). Our studies have shown that the specific docking of Far1 by Cln complexes involves other unique docking mechanisms (Valk & Loog, manuscript in preparation).

Intriguingly, the exclusive Clb5-specificity was dependent on the conserved *hp* docking pocket on cyclin (**Fig. 1H; Suppl. Fig. 2A**). We have previously shown that conventional RxLxF cyclin docking motifs usually enhance the specificity of targets via binding into the cyclin *hp* pockets of different cyclins, showing a trend of compensating the gradually weakening specificity towards the consensus phosphorylation peptide (k_{cat}/K_M: Clb2>Clb3>Clb5), and thereby, stronger relative docking effect for Clb5, intermediate for Clb3 and only few-fold for Clb2 (Kõivomägi et al., 2011a). More recently, we have shown that the *hp* pocket of different Clbs can accommodate exclusively specific non-RxL motifs, like an LxF motif for M-phase cyclin Clb2 and PxxPxF motif for G2-specific Clb3 (Örd et al., 2019a). In this respect, the Clb5-specific motif described in the current study falls into the latter category, being exclusively specific only for a particular cyclin while using the hydrophobic docking pocket conserved in Clb cyclins.

Substitution of the NLxxxL motif with an RxL results in partial loss of function

Having found that NLxxxL is an *hp*-binding motif like RxL, we asked if the two motifs have other functional differences in addition to the exclusive Clb5-specificity of NLxxxL. For this, we replaced the NLxxxL motif in 1-150-Far1 threshold sensor with an RxL motif from Sic1 (**Fig. 2A, Suppl. Fig. 2B**). Substitution of NLxxxL with an RxL motif caused a minor 3-minute delay in degradation, whereas the sensor with mutated RxL motif was degraded around 30 minutes later (**Fig. 2B, Suppl. Fig. 2C**), similarly to sensors with mutations in the NLxxxL determinants (**Fig. 1F**). To directly analyze the phosphorylation kinetics of 1-150-Far1 with the different docking motifs, we performed an *in vitro* steady-state kinase assay with Clb5-Cdk1. This revealed that K_M for 1-150-Far1 with NLxxxL motif is around 1.5 μM, and that substitution of NLxxxL with RxL increased K_M to 10 μM (**Fig. 2C**). The higher binding affinity in combination with slightly higher kcat results in around 13-fold higher specificity of the substrate with NLxxxL motif compared to the one with RxL. Interestingly, however, this large difference in specificity only results in a minor difference in phosphorylation timing (**Fig. 2B**). This suggests that extensive changes in specificity are needed to precisely order phosphorylation events at the onset of S phase due to the drastic increase in Cdk1 activity mediated by the activation of S-Cdk1 (Örd et al., 2019b).

To further analyze the functional differences of the two motifs, we tested the importance of the docking motif on the negative feedback loop of Far1 and Clb5-Cdk1 using a halo assay for pheromone sensitivity combined with overexpression of Clb5. Overexpression of Clb5 causes lethality in *sic1Δ* background (Jacobson et al., 2000), presumably due to inhibition of replication

origin licensing by Clb5-Cdk1 activity (Lengronne and Schwob, 2002). Activation of Far1, however, rescues the effect of Clb5 overexpression in *sic1 Δ* cells by inhibition of the excess Clb5-Cdk1 activity, thus enabling the cells to grow only in the presence of pheromone (**Fig. 2D**). Disruption of the NLxxxL docking by L135A mutation decreases the ability of the Clb5 overexpressing cells to grow in the presence of pheromone, as the cells grow in only a specific range of pheromone concentration (**Fig. 2D, Suppl. Fig. 2D**). This could be because of the inability to degrade Far1 in these cells. Furthermore, substitution of the NLxxxL motif with RxL motif results in a similar phenotype as L135A mutation, showing that RxL cannot substitute for NLxxxL motif in this case.

The contribution of Cks1 to the degron phosphorylation depends on the cyclin docking motif

In our previous studies of multisite phosphorylation of a number of key Cdk1 targets including Sic1, Cdc6, Swe1, Ndd1, and others, we have described a general mechanism of Cks1-mediated N-to-C terminally directed sequential phosphorylation process that can have varied degrees of processivity (Kõivomägi et al., 2011b, 2013; McGrath et al., 2013; Örd et al., 2019a). To study how the Cks1 docking affected phosphorylation of 1-150-Far1, we mutated the TP sites to SP (**Fig. 3A**), as only phospho-threonines bind to Cks1 (Kõivomägi et al., 2013; McGrath et al., 2013), and analyzed the degradation of the substrates using microscopy. Disconnection of Cks1 docking caused a 6-minute delay in sensor degradation (**Fig. 3B, Suppl. Fig. 3A**), indicating that Cks1 promotes the degron phosphorylation. Interestingly, the delay in degradation caused by mutation of Cks1 binding sites was greater in 1-150-Far1 constructs in which the NLxxxL motif was replaced with an RxL motif or which had no cyclin docking motif (**Fig. 3B, Suppl. Fig. 3A**). This indicates that the Cks1-dependence of the substrate phosphorylation also depends on the cyclin docking motif.

Mutation of both cyclin and Cks1 docking led to stabilization of the sensor to a similar extent as mutation of the degron (**Fig. 1D, 3B**), showing that the docking mechanisms are essential for phosphorylation of the output sites. This supports a previously suggested mechanism by which helper networks of Cks1 binding sites and cyclin docking motifs can enhance phosphorylation of output sites to time the phosphorylation to a specific point in the cell cycle (Örd et al., 2019b).

Analysis of the phosphorylation reactions using Phos-tag SDS-PAGE revealed that 1-150-Far1 is strongly multi-phosphorylated by Clb5-Cdk1, and that the appearance of highly multi-phosphorylated forms is Cks1-dependent also with the NLxxxL docking motif (**Fig. 3C, Suppl. Fig. 3B**). Substitution of NLxxxL motif with RxL results in a significant decrease in total phosphorylation rate, but has a lesser impact on the phosphorylation pattern compared to mutation of Cks1 binding sites (**Fig. 3C, Suppl. Fig. 2A, 3B**). Interestingly, despite the notable differences in phosphorylation rate, the 1-150-Far1(RxL) is degraded earlier *in vivo* compared to the WT SP mutant (**Fig. 3B, Suppl. Fig. 3A**), showing the importance of proper docking interactions in phosphorylation of the output sites. In case of 1-150-(Far1 RxL SP), both higher affinity cyclin docking and Cks1-mediated connections are lost, and this results in decreased accumulation of multi-phosphorylated forms and delayed sensor degradation (**Fig. 3B, C, Suppl. Fig. 3A, B**).

To study the Cks1-dependence in a minimal system, we deleted the region N-terminal of the degron (positions 1-85, **Fig. 3D**) and tested how introduction of a single optimal Cks1 priming site (based on Far1 T3) affects the degradation dynamics of substrates with different cyclin docking motifs. The deletion of positions 1-85 had only a minor effect in case of NLxxxL docking motif, and addition of T3 priming site did not improve the degradation (**Fig. 3E, F**). In case of either RxL or the absence of cyclin docking motif, deletion of the N-terminal region caused a major delay in degradation, which was rescued by introduction of Cks1 priming site (**Fig. 3E, F**). This shows that via NLxxxL docking, Clb5-Cdk1 is capable of efficiently phosphorylating the degron consisting of a minimal consensus (S87) and a non-proline site (S91), whereas with RxL docking these thresholds are not reached. Interestingly, this difference between the motifs could make some S phase targets

dependent on priming by other kinases, such as G1-CDK. Additionally, as NLxxxL docking enables direct phosphorylation of the degron, it could make phosphorylation of such substrates less sensitive to phosphatase activity.

Kinetic analysis of 85-150-Far1, a protein lacking 5 N-terminal phosphorylation sites and therefore also Cks1 binding sites revealed a slight increase in Km compared to 1-150-Far1 with NLxxxL docking site, and a stronger increase in case of RxL motif (**Fig. 2C, 3D**). Importantly, this confirms the significant difference in binding affinity of the NLxxxL and RxL motifs.

Modularity of the Far1 NLxxxL motif

In order to test if the identified linear docking motif is modular, and transferable between CDK targets without losing its function, we introduced the 9 amino acid segment (AT**NL**TTS**L**L) containing the motif from Far1 into a model substrate Sic1ΔC, as a replacement for a segment containing an RxL docking site characterized by us previously (**Fig. 4A**) (Örd et al., 2019b). Unexpectedly, degradation of this Sic1ΔC-GFP-based construct was very inefficient, reaching its half maximum only slightly earlier than the control sensor with no docking site at all, at ~55-60 minutes (**Fig. 4B, C**). The construct with intact RxL motif showed degradation half-life much earlier, at around ~30 minutes. However, when we introduced a longer version of the NLxxxL motif that also included the 4 amino acids from the C-terminal flanking segment (AT**NL**TTS**L**LRESI) (**Suppl. Fig. 4A**), a striking effect on degradation was observed, shifting the half-time to ~23 minutes after the *Start*. Interestingly, the C-terminal flanking residues (RESI) from the core motif NLxxxL did not affect the degradation of the sensor in Far1 context, while it was required for fast degradation within the Sic1-based construct. Latter difference was corroborated also in *in vitro* phosphorylation assay (**Suppl. Fig. 4B**). We can speculate that although the modular replacement of the docking motif from one substrate into the other was successful, there are apparently other weaker specificity elements in the local sequence context that may become more important if the module is replaced into foreign sequence context.

The Sic1-based sensor with the extended NLxxxL module was degraded even more rapidly than the construct with a native RxL motif from Sic1 (**Fig. 4B, C**). However, an *in vitro* phosphorylation assay similar kinetics for the substrates with either docking motifs (**Fig. 4D**). On the other hand, a high-resolution Phos-Tag SDS-PAGE assay providing the quantitative profiling of multi-phosphorylated species showed that the total signal of the most highly phosphorylated form was higher in case of the NLxxxL substrate (**Fig. 4E**). Furthermore, the relative quantitative pattern of multiply phosphorylated species was more shifted towards higher bands in case of NLxxxL compared to RxL (**Fig. 4F**). This result explains faster degradation timing of NLxxxL substrate, as efficient multi-site phosphorylation of Sic1 is essential for Sic1 degradation (Kõivomägi et al., 2011b).

Homology of the NLxxxL and RxL motifs

We performed a search for potential NLxxxL motifs from the intrinsically disordered proteins in yeast and found that the consensus sequence is present in 300 proteins, 50 of which have been previously found to be Cdk1 targets (**Supplementary Table 1**) and four of these (Lif1, Fin1, Yen1, Sld3) have been identified as physical interactors of Clb5 (Breitkreutz et al., 2010). We found that Lif1, a DNA ligase IV complex component functioning in DNA repair that is phosphorylated in S phase (Matsuzaki et al., 2012), is a specific target of Clb5-Cdk1 (**Fig. 5A**). Furthermore, phosphorylation of Lif1 was dependent on functional *hp* of Clb5 and an NLxxxL motif in Lif1 (**Fig. 5A, B**). This shows that NLxxxL controls the phosphorylation timing of other Cdk1 targets.

Surprisingly, we found that the consensus sequence for NLxxxL overlaps with previously described RxL motifs from Clb5-specific targets Fin1 and Spc110 (**Fig. 5A**). This gives rise to a hypothesis that the two motifs are homologous and have evolved slightly different binding modes to the cyclin *hp*, as the key residues in the interaction are different. Interestingly, an alignment of the

Fin1 ^{194}KNLLVEL motif within yeast species reveals that the motif earlier thought to function as an RxL motif could also be an NLxxxL motif, as the NLxxxL determinants are conserved, whereas the R/K of RxL has been lost in some species (**Suppl. Fig. 5A**). This indicates that the NLxxxL motifs could be derived from RxL motifs, as they can overlap, but by losing the RxL determinants can create a highly Clb5-specific docking motif. Whereas Fin1 homologs have uniform conservation of the NLxxxL consensus, Far1 and Lif1 homologs show higher diversity, with some homologs having either NLxxxL or RxL motif consensus sequences and some no carrying no known docking site in the region (**Suppl. Fig. 5B, C**). To test the functionality of the overlapping motifs in Fin1, we introduced single mutations to the docking region in Fin1 and analyzed phosphorylation of these substrates by Clb5-Cdk1 *in vitro*. Mutation of K194, a determinant of RxL motif, caused only a two-fold decrease in phosphorylation rate, whereas mutation of N195 and L200, the NLxxxL determinants resulted in greater decrease (**Fig. 5D**). Mutation of L196, however, had the greatest effect, likely because L196 is a determinant for both RxL and NLxxxL, indicating that both motifs have retained their functionality in Fin1.

To understand the overlap of the two motifs better, we introduced the RxL motif determinants to Far1 NLxxxL motif in Far1(1-150) mutant, where all TP sites have been mutated to SP sites (**Fig. 5E, F**). Mutation of the threonines to serines increases the CDK threshold, making timely phosphorylation more dependent on cyclin docking (**Fig. 3B**). Adding the RxL determinants to the NLxxxL motif, thus creating overlapping motifs **KNL**TTS**L** and **RNLF**TS**L**, did not significantly affect the timing of degradation (**Fig. 5G, H**). However, when the NLxxxL motif was substituted with conventional RxL motifs PKKLQF and PRKLQF, the degradation was delayed (**Fig. 5G, H**), confirming the stronger phosphorylation potentiation by the NLxxxL motif. Interestingly, the degradation of the sensor with PRKLQF took place around 20 minutes earlier than with PKKLQF. This corresponds with higher specificity of the PRKLQF motif and illustrates how cyclin docking motif affinity can affect the timing of phosphorylation throughout the cell cycle.

Clb5-specific docking motifs facilitate anaphase-specific dephosphorylation

RxL motifs that are exclusively specific to S-CDK could be important for assigning the timing of dephosphorylation to metaphase, as Clb5 is degraded before the metaphase-anaphase transition, while Clb2 is degraded in anaphase (Lu et al., 2014). To further analyze the temporal order of cyclin degradation, we performed time-lapse fluorescence microscopy with strains expressing B-type cyclins tagged with Citrine. For a reference, the 50% nuclear import time-point of Whi5-mCherry was used, which we determined to take place at about 14 minutes after anaphase onset (**Suppl. Fig. 6A**). The data confirmed that Clb5 degradation is complete at the onset of anaphase, while Clb2 and Clb1 are degraded over 20 minutes later (**Fig. 6A, B**). The quantitative model of CDK function states that as the CDK activity rises during the cell cycle, different activity thresholds are reached (Coudreuse and Nurse, 2010; Stern and Nurse, 1996). In metaphase-anaphase, the sequential degradation of cyclins leads to decrease in total CDK activity and ordered dephosphorylation of targets (Touati et al., 2018). Without cyclin specificity, the phosphorylation switches would occur in the last-in-first-out (LIFO) order, as the highest CDK thresholds met during the accumulation are also the first to be switched off in anaphase (**Fig. 6C**). The different docking specificity and degradation profiles of cyclins might influence the order of dephosphorylation in mitotic exit, creating the possibility for first-in-first-out (FIFO) switches (**Fig. 6C**).

We found that a group of Cdk1 targets that are dephosphorylated in anaphase (Bock et al., 2012; Liang et al., 2013; Woodbury and Morgan, 2007) contain the identified Clb5-specific motifs (**Fig. 6D**). We analyzed the cyclin specificity of phosphorylation of these substrates and confirmed that as predicted, Fin1, Spc110 and Cnn1 are most efficiently phosphorylated by S-CDK (**Fig. 6E, Suppl. Fig. 6B**), however, as these targets contained also other potential docking and phosphorylation motifs, the exclusive Clb5-specificity was not as pronounced as in minimal

constructs shown in three last lanes in Figure 6e. Fin1 is an intermediate filament protein that is phosphorylated by Clb5-Cdk1 and localizes to the nucleoplasm in metaphase, and following dephosphorylation at the onset of anaphase, is localized to the SPBs and the spindle (Woodbury and Morgan, 2007). We set out to analyze if the exclusively Clb5-specific RxL motif determined the timing of Fin1 dephosphorylation. For this, we replaced the RxL motif in Fin1 (G**K**N**L**LV) with an RxL motif that promotes phosphorylation also by Clb3- and Clb2-Cdk1 (P**K**K**L**QF). To study the dephosphorylation dynamics of Fin1 in an unperturbed cell cycle, we measured the accumulation of GFP-Fin1 to the SPBs relative to the onset of anaphase, as detected by Spc42-mCherry tagged SPBs (**Fig. 6F**). Wild-type Fin1 started accumulating at the SPBs at the time of spindle elongation, as published previously (**Fig. 6F, G**, (Woodbury and Morgan, 2007)). Fin1 with a P**K**K**L**QF RxL motif, however, showed a delay in SPB localization, suggesting that Fin1(PKKLQF) is dephosphorylated later. This result demonstrates that different RxL motifs may be used to assign different Cdk1 substrate dephosphorylation timings in anaphase. Importantly, previous studies have shown that while dephosphorylation of Fin1 is dependent on Clb5 degradation, dephosphorylation of Orc6 is not and occurs in later anaphase (Touati et al., 2018). While both Fin1 and Orc6 contain RxL motifs, the Orc6 RxL motif (R**R**K**L**AF) matches the consensus for conventional RxL motif promoting phosphorylation by Clb5- as well as Clb3- and Clb2-Cdk1. Therefore, the cyclin docking specificity might add another level of complexity to the dephosphorylation timing of CDK substrates in mitotic exit and facilitate mixed LIFO and FIFO switching orders (**Fig. 6C**).

Discussion

Our work sheds further light to previously less appreciated function of cyclins as versatile targeting scaffolds binding a wide range of short linear motifs in CDK substrate proteins. In fact, it has been a longstanding enigma, why evolution has chosen large proteins, whose costly synthesis and degradation cycle temporally activates CDK kinase domains. In fact, there are plenty of alternative and less costly ways to temporally and reversibly activate kinases by upstream signals, like phosphorylation or small second messenger accumulation.

Recent studies have revealed that cyclins have both common and exclusive substrate docking interactions. For example, RxLxF motif promotes phosphorylation by S-, G2- and M-Cdk1 complexes. Such motifs can establish a LIFO switching order, which could be necessary for example to avoid re-replication by keeping the proteins controlling replication licensing phosphorylated and inactivated from the start of S phase till the inhibition of Cdk1 activity in late mitosis. Alternatively, there are exclusively cyclin-specific motifs, like NLxxxL presented in this study, and LP, PxF, LxF for G1-, G2- and M-CDK, respectively (Bhaduri and Pryciak, 2011; Kõivomägi et al., 2011a; Örd et al., 2019a, 2019b). The motifs with exclusive specificity provide greater flexibility in temporal ordering of Cdk1 phosphorylation events.

In addition to triggering cell cycle events by Cdk1-mediated phosphorylation during the accumulation of cyclins, the temporal ordering of late mitotic events is also governed by dephosphorylation on specific targets (Kataria et al., 2018). As Clb5 is degraded prior to anaphase and the NLxxxL motif was predicted in several proteins that are dephosphorylated in early anaphase, the exclusively S-CDK-specific docking may have evolved to promote earlier dephosphorylation and achieve more complexity of CDK function via FIFO switching order.

An important element revealed was the relationship between the Cks1-dependent sequential route and the cyclin docking mechanisms. In case of more efficient docking, the Cks1 path was non-essential for fast degradation, while in case of weaker docking, like demonstrated by the RxL in Far1 context, the path became essential. Highly efficient NLxxxxL is alone sufficient for degron phosphorylation and promotes processive phosphorylation. These differences in affinity could

contribute to finetuning of S phase phosphorylation and in some cases could also affect the contribution of phosphatases and other priming kinases to the phosphorylation switch.

In conclusion, cyclins will most certainly provide more SLiMs with various binding modes to facilitate substrate and inhibitor protein binding at a wide range of affinities. Cyclin surfaces as scaffolds for various SLiMs is a new look at the function of CDK complexes. There are many things still to be discovered conserving the joint action of Cks1 and the docking motifs and what distinguishes the substrates from inhibitors.

Materials and Methods

Yeast strains

S. cerevisiae strains were of W303 background and are described in Supplementary Table 1. Gene deletions and mutations, promoter substitutions and tagging were carried out using PCR-based homologous recombination (Janke et al., 2004; Longtine et al., 1998). All gene modifications were confirmed by DNA sequencing. Far1(1-150) constructs were cloned into pRS306 vector containing *SIC1* promoter (1-420 base pairs upstream of *SIC1* gene) and C-terminal EGFP. The vectors were linearized and integrated to *URA3* locus. The transformants were selected for single-copy integration by fluorescence intensity.

Time-lapse fluorescence microscopy

Cells were grown at 30 °C in synthetic complete media with 2% glucose (SC) to OD 0.2–0.6 before the experiment. Cells were then pipetted onto 0.8-mm cover glass and covered with a 1-mm thick 1.5% SC/glucose agarose pad (NuSieve™ GTG™ Agarose, Lonza). Cells were incubated under the agarose pad for 1 hour before the start of the experiment. Imaging was executed using a Zeiss Observer Z1 microscope with a 63×/1.4NA oil immersion objective and Axiocam 506 mono camera (Zeiss), using 3×3 binning. The sample was kept at 30 °C using Tempcontrol 37–2 digital (PeCon). Cells were imaged every 3 min, except for experiments with GFP-Fin1 Spc42-mCherry, where images were taken every 2 min. The experiments were 8 h long and contained up to 12 positions that were followed using an automated stage and ZEN software (Zeiss). Focus was kept using Definite Focus. Colibri 470 LED module with exposure time of 15 ms was used for excitation of EGFP-tagged proteins. Excitement of cyclins fused with yeCitrine was performed using a Colibri 505 LED module for 500 ms. Whi5-mCherry was excited using Colibri 540–580 LED module for 750 ms. All Colibri modules were used at 25% power. Filter set 72 HE (Zeiss) was used for imaging EGFP and mCherry, and filter set 61 HE (Zeiss) was used for yeCitrine.

Image segmentation, cell tracking, and quantification of fluorescence signals was performed using MATLAB (The MathWorks, Inc.) as described in (Doncic et al., 2013). All plots with microscopy data contain data from at least two experiments, the exact number of cells analyzed from each strain is presented in Supplementary Table 1.

Protein purification

Cdk1 substrate proteins were purified from *E. coli*. Far1(1-150)-EGFP, Sic1(1-215), Fin1, Cnn1 and Spc110 were N-terminally tagged with 6xHis tag and were expressed in BL21RP cells. Expression of Far1(1-150)-EGFP, Fin1, Cnn1 and Spc110 was induced with 0.3 mM IPTG at 16 °C, whereas Sic1(1-215) was induced with 1 mM IPTG at 37 °C. The proteins were purified using immobilized cobalt affinity chromatography and were eluted with imidazole.

Yeast cyclin-Cdk1 complexes were purified from S. cerevisiae cells where the tagged cyclin was overexpressed from *GAL1* promoter. Clb5, Clb3 and Clb2 were purified using the tandem affinity purification method (Puig et al., 2001; Ubersax et al., 2003). Cln2 with N-terminal 3HA tag was

purified as described (McCusker et al., 2007). Yeast cells were lysed using Mixer Mill MM 400 (Retch). Cks1 was expressed in *E. coli* BL21RP and purified as described (Reynard et al., 2000).

Kinase assay

The phosphorylation reactions were performed at room temperature in buffer containing 50 mM Hepes-KOH, pH 7.4, 150 mM NaCl, 5 mM $MgCl_2$, 20 mM imidazole, 2% glycerol, 0.2 mg/ml BSA, 500 nM Cks1 and 500 µM ATP [(with added [γ-^{32}P]-ATP (Hartmann Analytic)]. Substrate protein concentrations were 1 µM (in the linear [S] versus v0 range, several-fold below the estimated KM value) unless noted otherwise. The concentrations of kinase complexes were around 0.2 nM. The kinase assays were performed under conditions below 10% of initial substrate turnover. Reactions were stopped at two time points (8 and 16 minutes) with SDS-PAGE sample buffer and separated using SDS-PAGE.

γ-^{32}P phosphorylation signals were detected using an Amersham Typhoon 5 Biomolecular Imager (GE Healthcare Life Sciences). Signals were quantified using ImageQuant TL (Amersham Biosciences) and GraphPad Prism 5.0 was used for data analysis. All kinase assays were performed in at least two replicate experiments.

Pheromone sensitivity assay

Yeast cultures were grown in YPD to stationary phase. 10 µl of the culture was mixed with 0.5% agar and plated on YPD or YPG plate. Then, filter paper discs were placed on the plate and 1 µl of solution containing 0, 20 µg, 2 µg or 0.2 µg of α-factor in DMSO was pipetted on the discs. The plates were incubated at 30 °C for 1 or 2 days for YPD or YPG plates, respectively.

Bioinformatics

Potential NLxxxL motifs were searched from the intrinsically disordered regions (defined by positions with IUPRED score over 0.3) of *S. cerevisiae* proteome using SlimSearch4 (Krystkowiak and Davey, 2017).

Acknowledgements

We thank J. Mihhejev for excellent technical assistance. The work was funded by ERC Consolidator Grant 649124, Centre of Excellence for “Molecular Cell Technologies” TK143, and Estonian Science Agency grant PRG550 to M.L.

Author contributions

IF, MÖ and ML directed the study. IF, LB, FM, EV and MÖ cloned the constructs, made the yeast strains, and purified the proteins. IF, LB, FM and MÖ performed the experiments. MÖ and ML wrote the manuscript.

Declaration of Interests The authors declare no competing interests.

References

Bhaduri, S., and Pryciak, P.M. (2011). Cyclin-specific docking motifs promote phosphorylation of yeast signaling proteins by G1/S Cdk complexes. Curr. Biol. *21*, 1615–1623.

Bhaduri, S., Valk, E., Winters, M.J., Gruessner, B., Loog, M., and Pryciak, P.M. (2015). A docking interface in the cyclin Cln2 promotes multi-site phosphorylation of substrates and timely cell-cycle entry. Curr. Biol. *25*, 316–325.

Bock, L.J., Pagliuca, C., Kobayashi, N., Grove, R.A., Oku, Y., Shrestha, K., Alfieri, C., Golfieri, C.,

Oldani, A., Dal Maschio, M., et al. (2012). Cnn1 inhibits the interactions between the KMN complexes of the yeast kinetochore. Nat. Cell Biol. *14*, 614–624.

Breitkreutz, A., Choi, H., Sharom, J.R., Boucher, L., Neduva, V., Larsen, B., Lin, Z.Y., Breitkreutz,

B.J., Stark, C., Liu, G., et al. (2010). A global protein kinase and phosphatase interaction network in yeast. Science (80-.). *328*, 1043–1046.

Coudreuse, D., and Nurse, P. (2010). Driving the cell cycle with a minimal CDK control network. Nature *468*, 1074–1079.

Davey, N.E., Van Roey, K., Weatheritt, R.J., Toedt, G., Uyar, B., Altenberg, B., Budd, A., Diella, F., Dinkel, H., and Gibson, T.J. (2012). Attributes of short linear motifs. Mol. Biosyst. *8*, 268–281.

Doncic, A., Falleur-Fettig, M., and Skotheim, J.M. (2011). Distinct Interactions Select and Maintain a Specific Cell Fate. Mol. Cell *43*, 528–539.

Doncic, A., Eser, U., Atay, O., and Skotheim, J.M. (2013). An algorithm to automate yeast segmentation and tracking. PLoS One *8*, e57970.

Enserink, J.M., and Kolodner, R.D. (2010). An overview of Cdk1-controlled targets and processes. Cell Div. *5*, 11.

Holt, L.J., Tuch, B.B., Villén, J., Johnson, A.D., Gygi, S.P., and Morgan, D.O. (2009). Global analysis of Cdk1 substrate phosphorylation sites provides insights into evolution. Science *325*, 1682–1686.

Jacobson, M.D., Gray, S., Yuste-Rojas, M., and Cross, F.R. (2000). Testing Cyclin Specificity in the Exit from Mitosis. Mol. Cell. Biol. *20*, 4483–4493.

Janke, C., Magiera, M.M., Rathfelder, N., Taxis, C., Reber, S., Maekawa, H., Moreno-Borchart, A., Doenges, G., Schwob, E., Schiebel, E., et al. (2004). A versatile toolbox for PCR-based tagging of yeast genes: new fluorescent proteins, more markers and promoter substitution cassettes. Yeast *21*, 947–962.

Kataria, M., Mouilleron, S., Seo, M.-H., Corbi-Verge, C., Kim, P.M., and Uhlmann, F. (2018). A PxL motif promotes timely cell cycle substrate dephosphorylation by the Cdc14 phosphatase. Nat. Struct. Mol. Biol. *25*, 1093–1102.

Kõivomägi, M., Valk, E., Venta, R., Iofik, A., Lepiku, M., Morgan, D.O., and Loog, M. (2011a). Dynamics of Cdk1 Substrate Specificity during the Cell Cycle. Mol. Cell *42*, 610–623.
Kõivomägi, M., Valk, E., Venta, R., Iofik, A., Lepiku, M., Balog, E.R.M., Rubin, S.M., Morgan,

D.O., and Loog, M. (2011b). Cascades of multisite phosphorylation control Sic1 destruction at the onset of S phase. Nature *480*, 128–131.

Kõivomägi, M., Örd, M., Iofik, A., Valk, E., Venta, R., Faustova, I., Kivi, R., Balog, E.R.M., Rubin, S.M., and Loog, M. (2013). Multisite phosphorylation networks as signal processors for Cdk1. Nat. Struct. Mol. Biol. *20*.

Krystkowiak, I., and Davey, N.E. (2017). SLiMSearch: a framework for proteome-wide discovery and annotation of functional modules in intrinsically disordered regions. Nucleic Acids Res. *45*, W464–W469.

Lengronne, A., and Schwob, E. (2002). The yeast CDK inhibitor Sic1 prevents genomic instability by promoting replication origin licensing in late G1. Mol. Cell *9*, 1067–1078.

Liang, F., Richmond, D., and Wang, Y. (2013). Coordination of Chromatid Separation and Spindle Elongation by Antagonistic Activities of Mitotic and S-Phase CDKs. PLoS Genet. *9*, e1003319.

Longtine, M.S., Mckenzie III, A., Demarini, D.J., Shah, N.G., Wach, A., Brachat, A., Philippsen, P., and Pringle, J.R. (1998). Additional modules for versatile and economical PCR-based gene deletion and modification in Saccharomyces cerevisiae. Yeast *14*, 953–961.

Loog, M., and Morgan, D.O. (2005). Cyclin specificity in the phosphorylation of cyclin-dependent kinase substrates. Nature *434*, 104–108.

Lu, D., Hsiao, J.Y., Davey, N.E., Van Voorhis, V.A., Foster, S.A., Tang, C., and Morgan, D.O. (2014). Multiple mechanisms determine the order of APC/C substrate degradation in mitosis. J. Cell Biol. *207*, 23–39.

Matsuzaki, K., Terasawa, M., Iwasaki, D., Higashide, M., and Shinohara, M. (2012). Cyclin-dependent kinase-dependent phosphorylation of Lif1 and Sae2 controls imprecise nonhomologous end joining accompanied by double-strand break resection. Genes to Cells *17*, 473–493.

McCusker, D., Denison, C., Anderson, S., Egelhofer, T.A., Yates, J.R., Gygi, S.P., and Kellogg, D.R. (2007). Cdk1 coordinates cell-surface growth with the cell cycle. Nat. Cell Biol. *9*, 506–515.

McGrath, D.A., Balog, E.R.M., Kõivomägi, M., Lucena, R., Mai, M. V, Hirschi, A., Kellogg, D.R., Loog, M., and Rubin, S.M. (2013). Cks confers specificity to phosphorylation-dependent CDK signaling pathways. Nat. Struct. Mol. Biol. *20*, 1407–1414.

Morgan, D.O. (2007). The cell cycle : principles of control (New Science Press).

Örd, M., and Loog, M. (2019). How the cell cycle clock ticks. Mol. Biol. Cell *30*, 169–172.

Örd, M., Venta, R., Möll, K., Valk, E., and Loog, M. (2019a). Cyclin-Specific Docking Mechanisms Reveal the Complexity of M-CDK Function in the Cell Cycle. Mol. Cell *75*, 76-89.e3.

Örd, M., Möll, K., Agerova, A., Kivi, R., Faustova, I., Venta, R., Valk, E., and Loog, M. (2019b). Multisite phosphorylation code of CDK. Nat. Struct. Mol. Biol. *26*, 649–658.

Puig, O., Caspary, F., Rigaut, G., Rutz, B., Bouveret, E., Bragado-Nilsson, E., Wilm, M., and Séraphin, B. (2001). The Tandem Affinity Purification (TAP) Method: A General Procedure of Protein Complex Purification. Methods *24*, 218–229.

Reynard, G.J., Reynolds, W., Verma, R., and Deshaies, R.J. (2000). Cks1 is required for G(1) cyclin-cyclin-dependent kinase activity in budding yeast. Mol. Cell. Biol. *20*, 5858–5864.

Russo, A.A., Jeffrey, P.D., Patten, A.K., Massagué, J., and Pavletich, N.P. (1996). Crystal structure of the p27(Kip1) cyclin-dependent-kinase inhibitor bound to the cyclin A-Cdk2 complex. Nature *382*, 325–331.

Schulman, B.A., Lindstrom, D.L., and Harlow, E.D. (1998). Substrate recruitment to cyclin-dependent kinase 2 by a multipurpose docking site on cyclin A.

Stern, B., and Nurse, P. (1996). A quantitative model for the cdc2 control of S phase and mitosis in fission yeast. Trends Genet. *12*, 345–350.

Swaffer, M.P., Jones, A.W., Flynn, H.R., Snijders, A.P., and Nurse, P. (2016). CDK Substrate Phosphorylation and Ordering the Cell Cycle. Cell *167*, 1750-1761.e16.

Takeda, D.Y., Wohlschlegel, J.A., and Dutta, A. (2001). A bipartite substrate recognition motif for cyclin-dependent kinases. J. Biol. Chem. *276*, 1993–1997.

Topacio, B.R., Zatulovskiy, E., Cristea, S., Xie, S., Tambo, C.S., Rubin, S.M., Sage, J., Kõivomägi, M., and Skotheim, J.M. (2019). Cyclin D-Cdk4,6 Drives Cell-Cycle Progression via the Retinoblastoma Protein's C-Terminal Helix. Mol. Cell *0*.

Touati, S.A., Kataria, M., Jones, A.W., Snijders, A.P., and Uhlmann, F. (2018). Phosphoproteome dynamics during mitotic exit in budding yeast. EMBO J. *37*.

Ubersax, J.A., Woodbury, E.L., Quang, P.N., Paraz, M., Blethrow, J.D., Shah, K., Shokat, K.M.,

and Morgan, D.O. (2003). Targets of the cyclin-dependent kinase Cdk1. Nature *425*, 859–864.

Venta, R., Valk, E., Örd, M., Košik, O., Pääbo, K., Maljavin, A., Kivi, R., Faustova, I., Shtaida, N., Lepiku, M., et al. (2020). A processive phosphorylation circuit with multiple kinase inputs and mutually diversional routes controls G1/S decision. Nat. Commun. *11*, 1836.

Wilmes, G.M., Archambault, V., Austin, R.J., Jacobson, M.D., Bell, S.P., and Cross, F.R. (2004). Interaction of the S-phase cyclin Clb5 with an RXL docking sequence in the initiator protein Orc6 provides an origin-localized replication control switch. Genes Dev. *18*, 981–991.

Wohlschlegel, J.A., Dwyer, B.T., Takeda, D.Y., and Dutta, A. (2001). Mutational analysis of the Cy motif from p21 reveals sequence degeneracy and specificity for different cyclin-dependent kinases. Mol. Cell. Biol. *21*, 4868–4874.

Woodbury, E.L., and Morgan, D.O. (2007). Cdk and APC activities limit the spindle-stabilizing function of Fin1 to anaphase. Nat. Cell Biol. *9*, 106–112.

Zhou, P., and Howley, P.M. (1998). Ubiquitination and Degradation of the Substrate Recognition Subunits of SCF Ubiquitin–Protein Ligases. Mol. Cell *2*, 571–580.

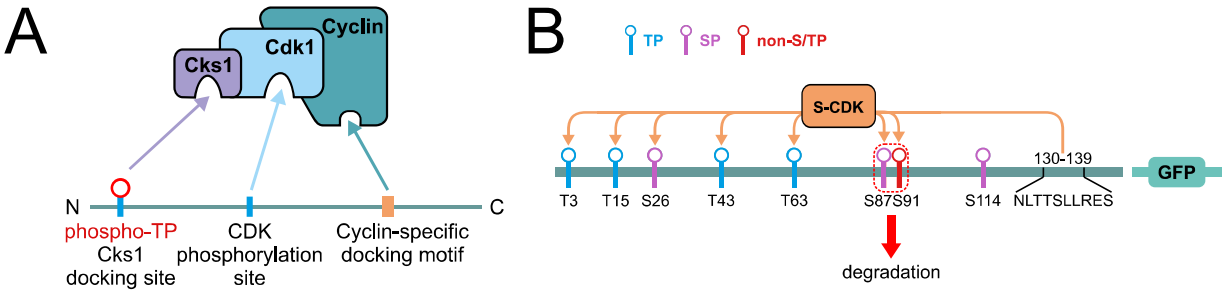

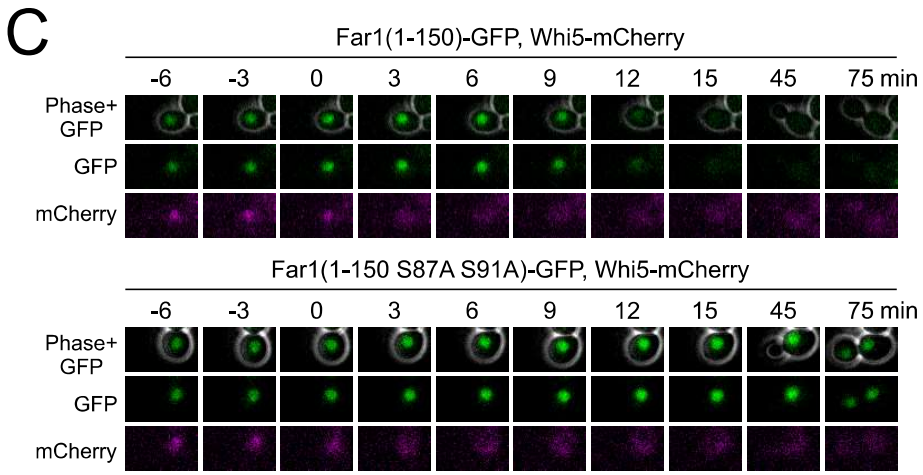

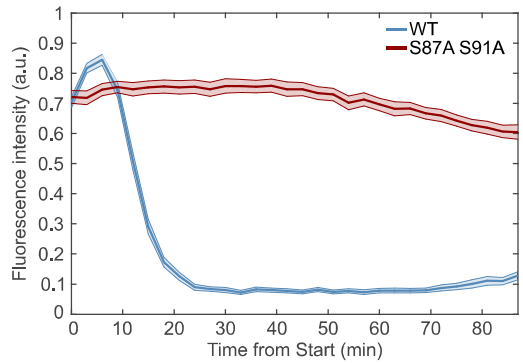

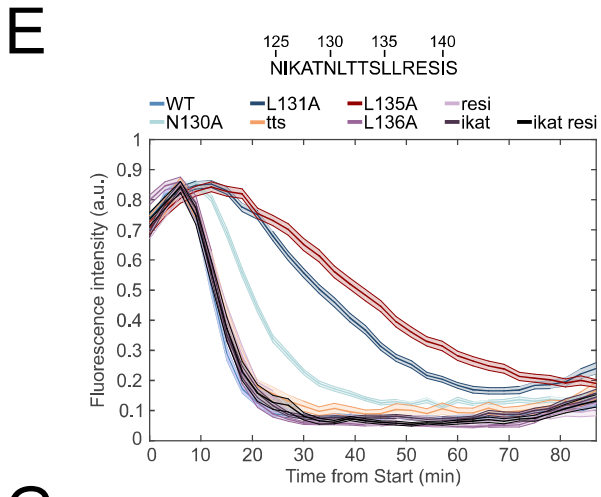

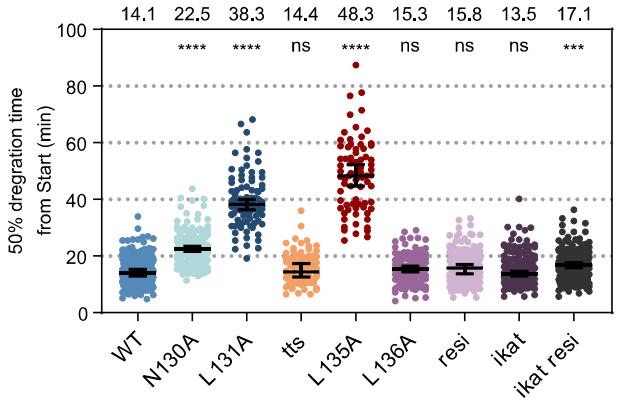

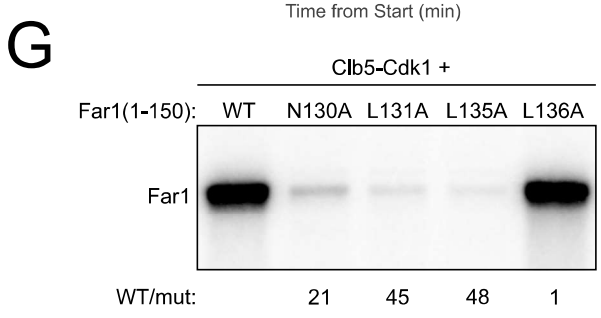

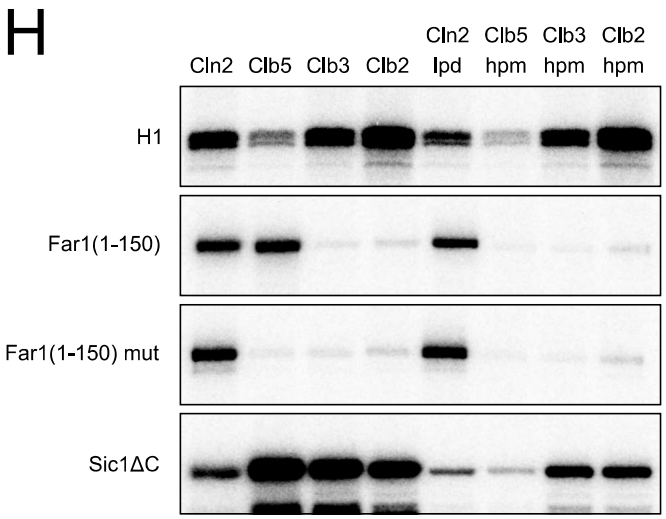

Figure 1. NLxxxL motif mediates Clb5-specific phosphorylation to promote degradation of N-Far1. (A) Scheme showing the major cyclin-substrate interactions of Cdk1 complex. (B) Scheme showing the CDK phosphorylation sites and the potential Clb5 docking region in the disordered N-terminus of Far1 (residues 1-150). (C) Time-lapse fluorescence images showing the expression and degradation of wild-type and S87A S91A mutant Far1(1-150)-GFP and nuclear-cytoplasmic shuttling of Whi5-mCherry. Nuclear export of Whi5-mCherry takes place at 0 min (Start point) and was used to synchronize the cells for quantitative analysis. (D, E) Mean±SEM fluorescence intensities of the indicated Far1(1-150)-GFP mutants over the cell cycle. (F) Time from Start to degradation of 50% of the indicated Far1-GFP sensor in single cells. The numbers above the plot show median values. **** indicates p-value <0.0001, * <0.05 and ns >0.05 for pair-wise comparisons with wild-type using Mann Whitney U test. (G) Autoradiograph of an in vitro kinase assay showing the effect of N130A, L131A, L135A and L136A mutations on Far1(1-150)-GFP phosphorylation by Clb5-Cdk1. WT/mut shows the decrease in phosphorylation rate of the mutant compared to wild-type. (H) Autoradiograph of a cyclin-specificity analysis of the indicated substrates with wild-type or docking site mutant cyclin-Cdk1 complexes. Far1(1-150 mut) is L131A L135A L136A mutant, Sic1ΔC is the non-inhibitory mutant of Sic1 (deletion of 216-284).

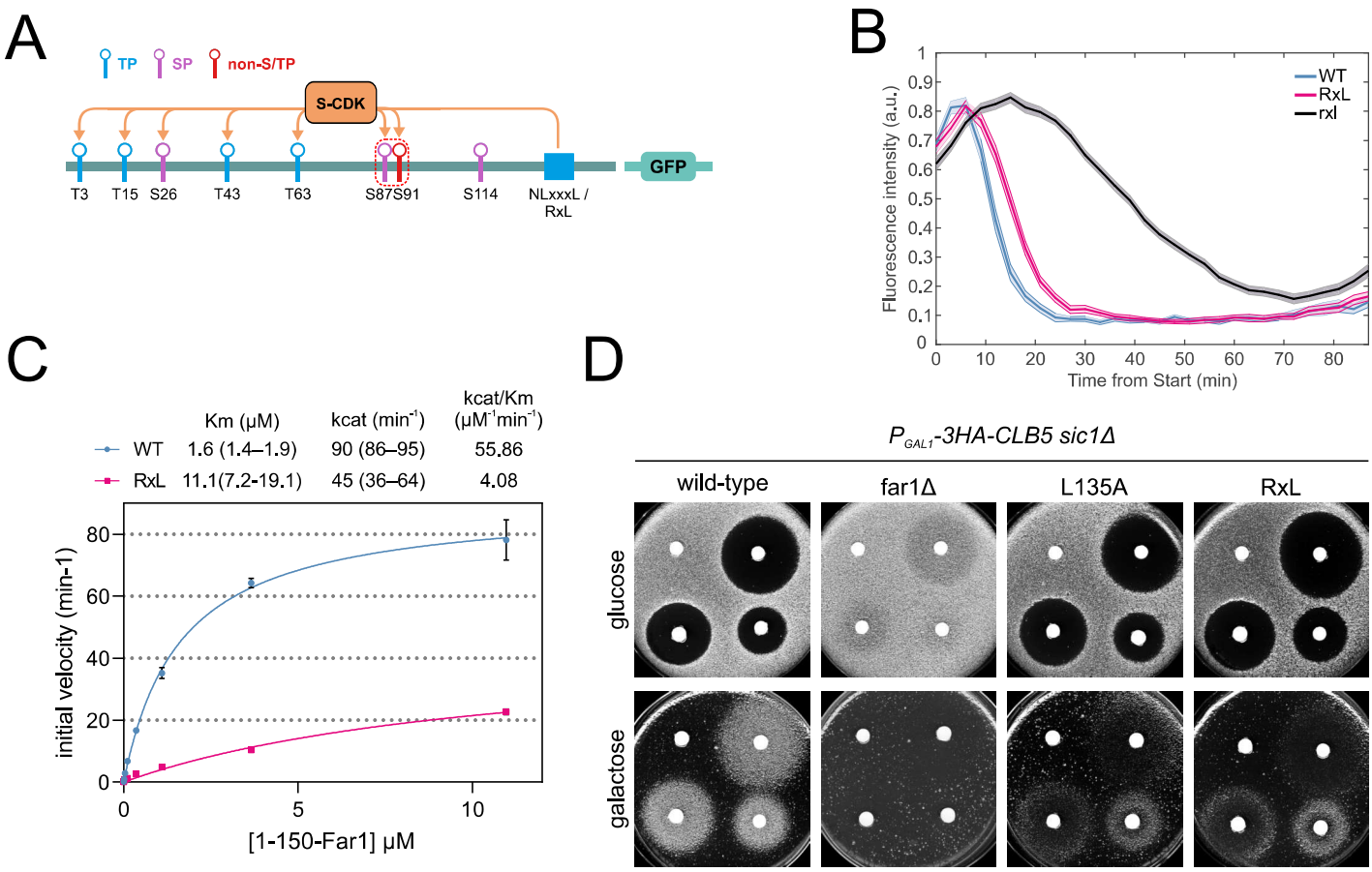

Figure 2. NLxxxL motif is more effective than RxL motif in directing Clb5-Cdk1 activity. (A) Schemes of Far1(1-150)-GFP constructs, either wild-type or mutant where NLxxxL motif is replaced with RxL motif (VK**R**T**LF**), that are used in time-lapse microscopy experiments in panel 'B'. (B) Plot showing the mean±SEM fluorescence intensities of Far1(1-150)-GFP constructs with the indicated docking site. In rxl mutant, the NLxxxL motif is replaced with a mutated non-functional RxL motif (VK**A**T**A**F). (C) Kinetic characterization of Far1(1-150 WT)-GFP and Far1(1-150 RxL)-GFP phosphorylation by Clb5-Cdk1. (D) Pheromone sensitivity halo assay with P_{GAL1}*-3HA-CLB5 sic1Δ* strains carrying either wild-type *FAR1*, *far1Δ*, *far1(L135A)* or *far1(RxL)*. Different concentrations of α-factor were pipetted on the paper discs.

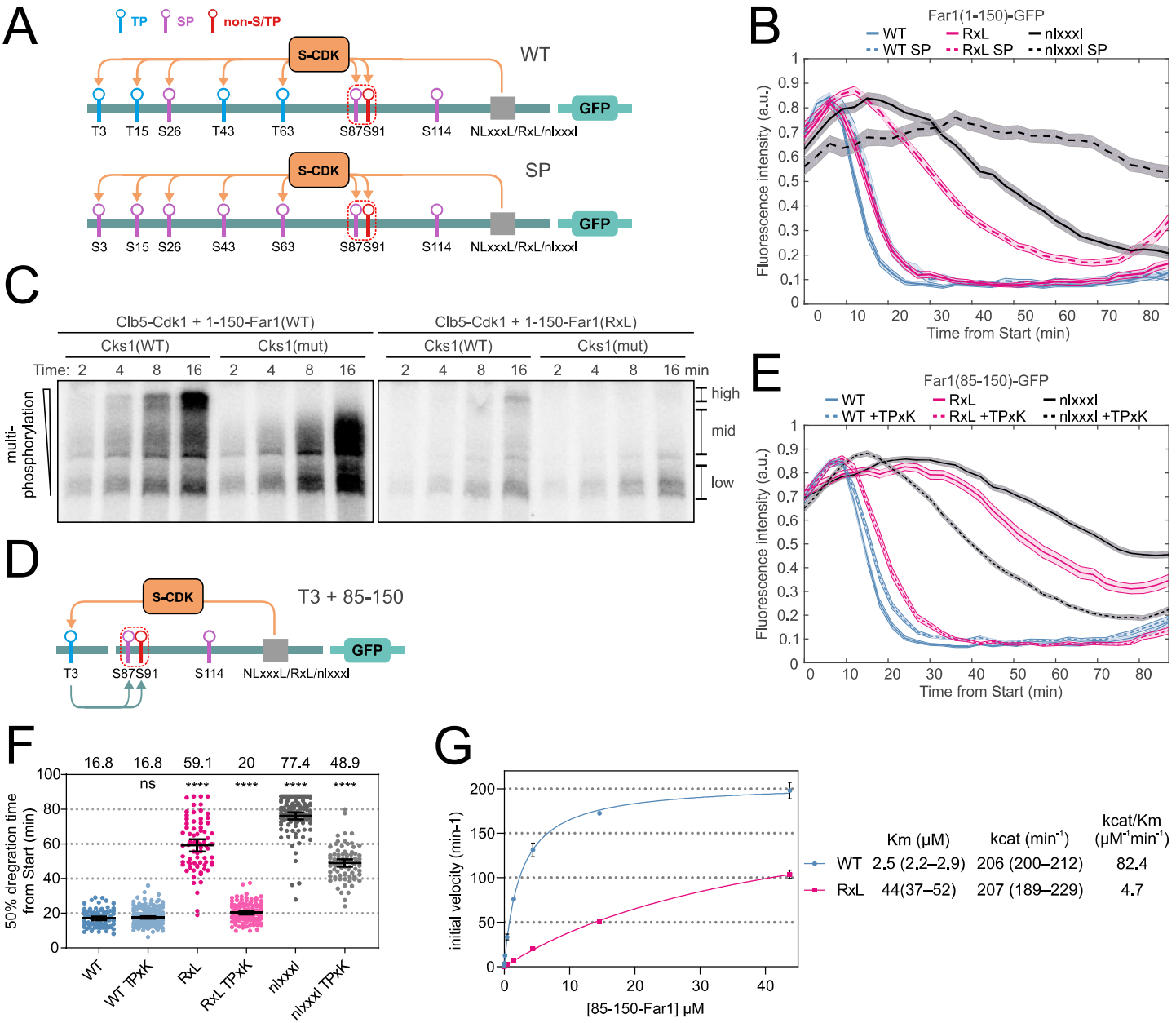

Figure 3. The Cks1-dependency is affected by the affinity of the cyclin docking motif. (A) Schemes of the Far1(1-150)-GFP constructs used in 'B'. The constructs contain either wild-type phosphorylation sites or have all TP sites mutated to SP sites (SP mutant). (B) The degradation of Far1(1-150)-GFP with either wild-type or all serine-based phosphorylation sites and the indicated docking motifs was measured in time-lapse microscopy. Plot shows mean±SEM of GFP fluorescence intensities from Start. (C) Phos-tag SDS-PAGE autoradiographs showing the Cks1-dependency of Clb5-Cdk1-mediated multisite phosphorylation of Far1(1-150) with either NLxxxL (WT) motif or RxL motif. (D) Scheme of Far1(85-150)-GFP with either NLxxxL, RxL or mutated cyclin docking motif and with or without T3 primer site introduced upstream of the S87 S91 degron. (E) Mean±SEM GFP fluorescence intensities of the indicated Far1(1-85) constructs, synchronized at the time of Start. (F) Plot showing the timing of 50% degradation of the indicated Far1(85-150) constructs in single cells. The error bars show median±95% CI. **** and ns indicate p-values <0.0001 and <0.05 by Mann-Whitney test for pair-wise comparisons with WT. (G) Plot showing the kinetics of Clb5-Cdk1-mediated phosphorylation of Far1(85-150) with either wild-type (NLxxxL) or RxL docking motif.

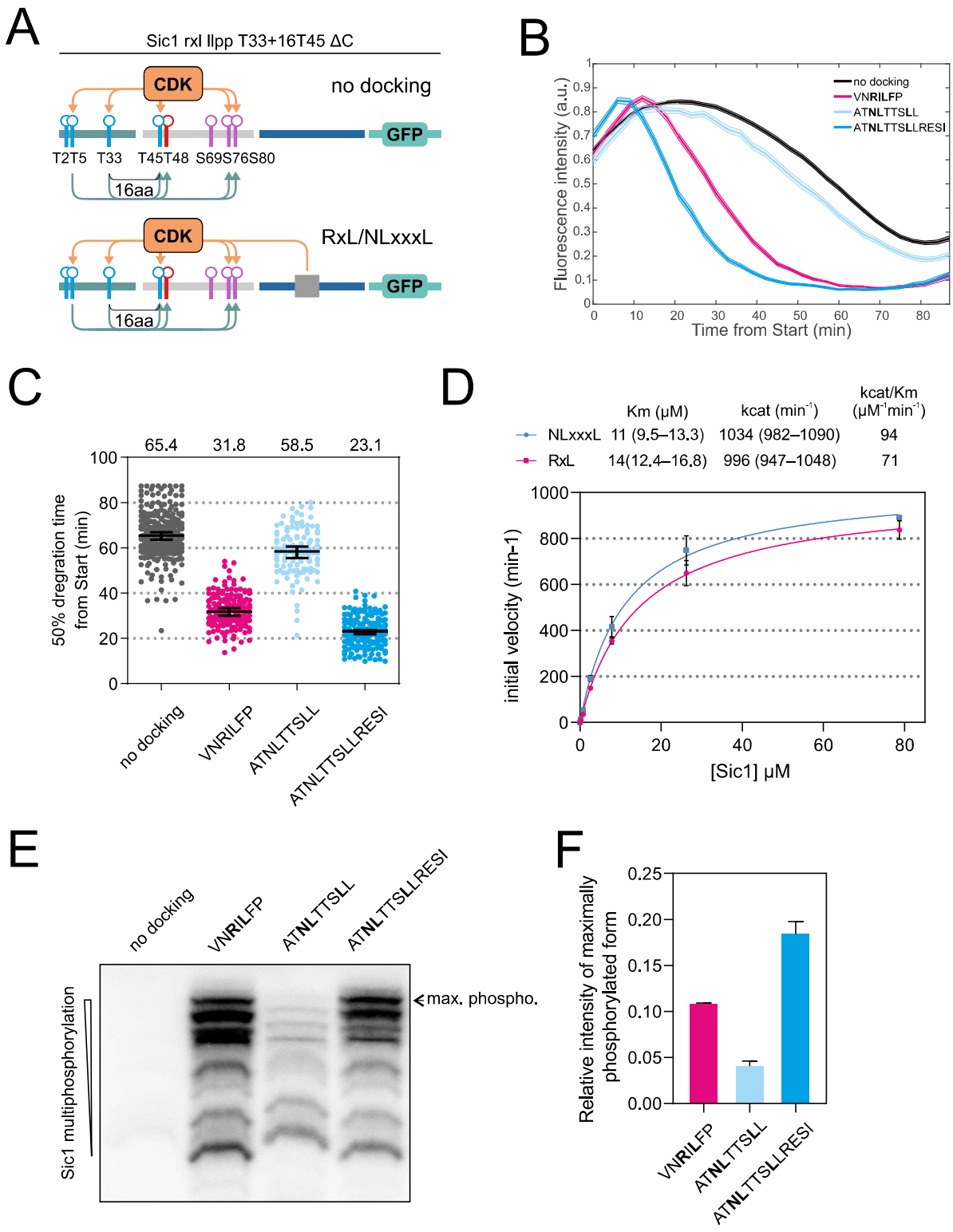

Figure 4. NLxxxL motif can substitute RxL in targeting Clb5-Cdk1 activity for degradation of Sic1. (A) Schemes of the CDK threshold sensors based on Sic1 used in panels 'B' and 'C'. The sensors contain the non-inhibitory domain of Sic1 (1-215), have mutated RxL and LP docking sites and insertion of 4 residues between T33 and T45. The docking sites are inserted to the position of Sic1 RxL motif (Suppl. Fig. 4A). (B) Plot showing the mean±SEM fluorescence intensities of the Sic1-based threshold sensors shown in 'A' containing the indicated cyclin docking motif. (C) The time from Start to the fluorescence levels of the threshold sensors with indicated docking motifs decreasing to 50% of peak level was measured in single cells. The black lines show median±95% CI. The numbers above the plot show median degradation timings of the indicated sensors. (D) In vitro phosphorylation kinetics of Sic1(T33+16T45 rxl llpp ΔC) with the indicated cyclin docking motif by Clb5-Cdk1. (E) Analysis of multisite phosphorylation of Sic1(T33+16T45 rxl llpp ΔC) with different docking motifs using Phos-tag SDS-PAGE autoradiography. (F) The fraction of maximally phosphorylated form from total phosphorylation signal was quantified from Phos-tag gels as shown in panel 'E'.

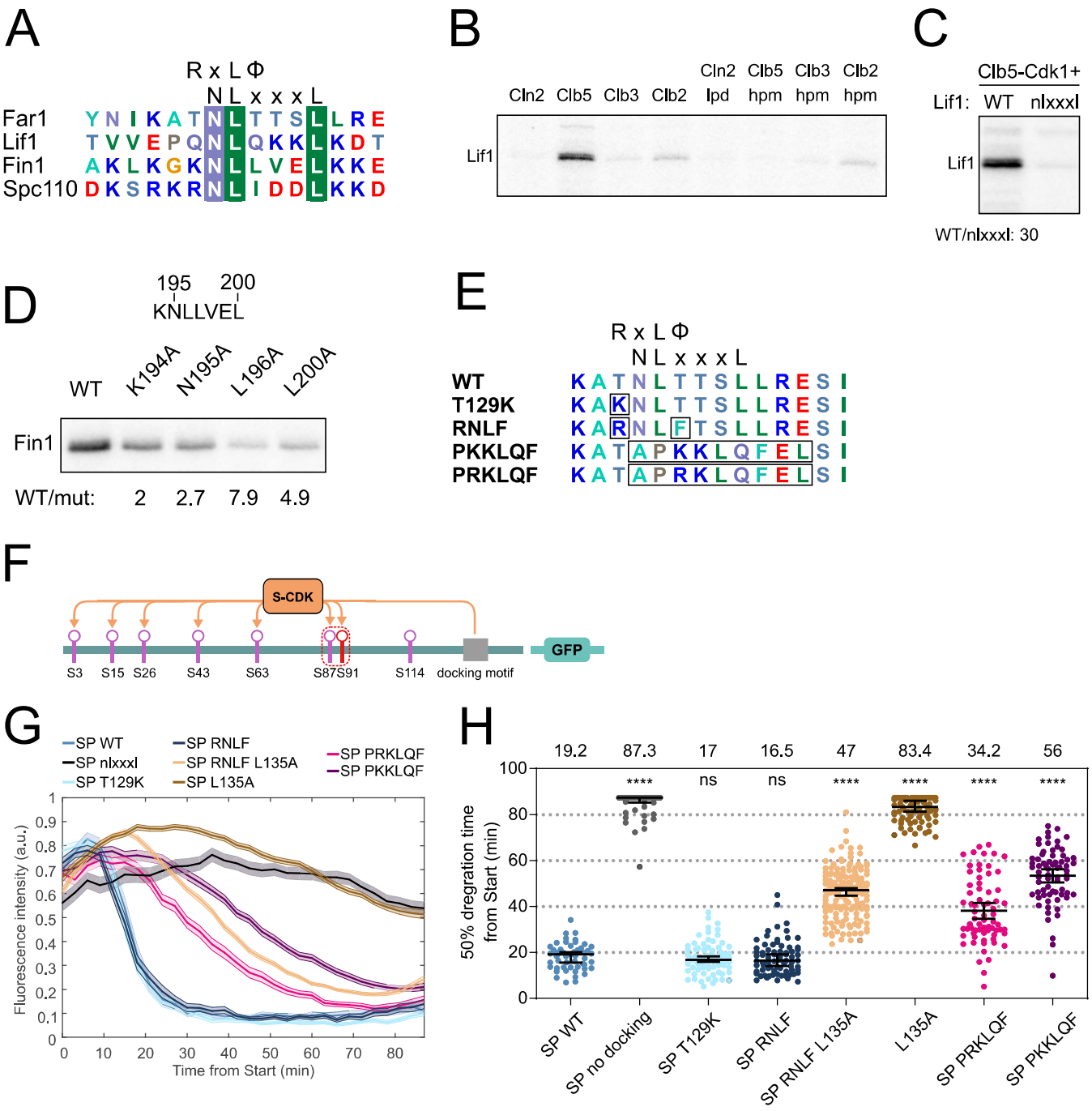

Figure 5. NLxxxL motif is present in other S-CDK targets and is homologous with RxL motif. (A) An alignment of predicted NLxxxL motifs from Far1, Lif1, Fin1 and Spc110. In case of Fin1 and Spc110, the motif overlaps with an RxL motif. (B) Autoradiograph showing the cyclin specificity and docking dependency of Lif1 phosphorylation. (C) NLxxxL is necessary for efficient Lif1 phosphorylation by Clb5-Cdk1, as shown by the autoradiograph of the *in vitro* kinase assay. (D) Autoradiograph of Clb5-Cdk1-mediated phosphorylation of indicated Fin1 mutants. (E) Alignment showing the introduction of RxL motif determinants to Far1 NLxxxL motif in mutants analyzed in time-lapse microscopy in panels 'G-H'. (F) Scheme of Far1(1-150 SP)-GFP sensors used for time-lapse microscopy-based analysis of different docking motif variants. All TP sites have been mutated to SP sites. (G) The effect of different docking motifs on the degradation of Far1(1-150 SP)-GFP, where all TP sites are mutated to SP. Plot shows mean±SEM of fluorescence intensities in the cell cycle. (H) The time from Start to the degradation of 50% of Far1(1-150 SP)-GFP with the indicated docking motif was measured in single cells. The numbers above the plot show median values for the sensors, the black lines show median±95% CI. **** and ns denote p-value <0.0001 and >0.05, respectively, for pair-wise comparisons with SP WT using Mann-Whitney U test.

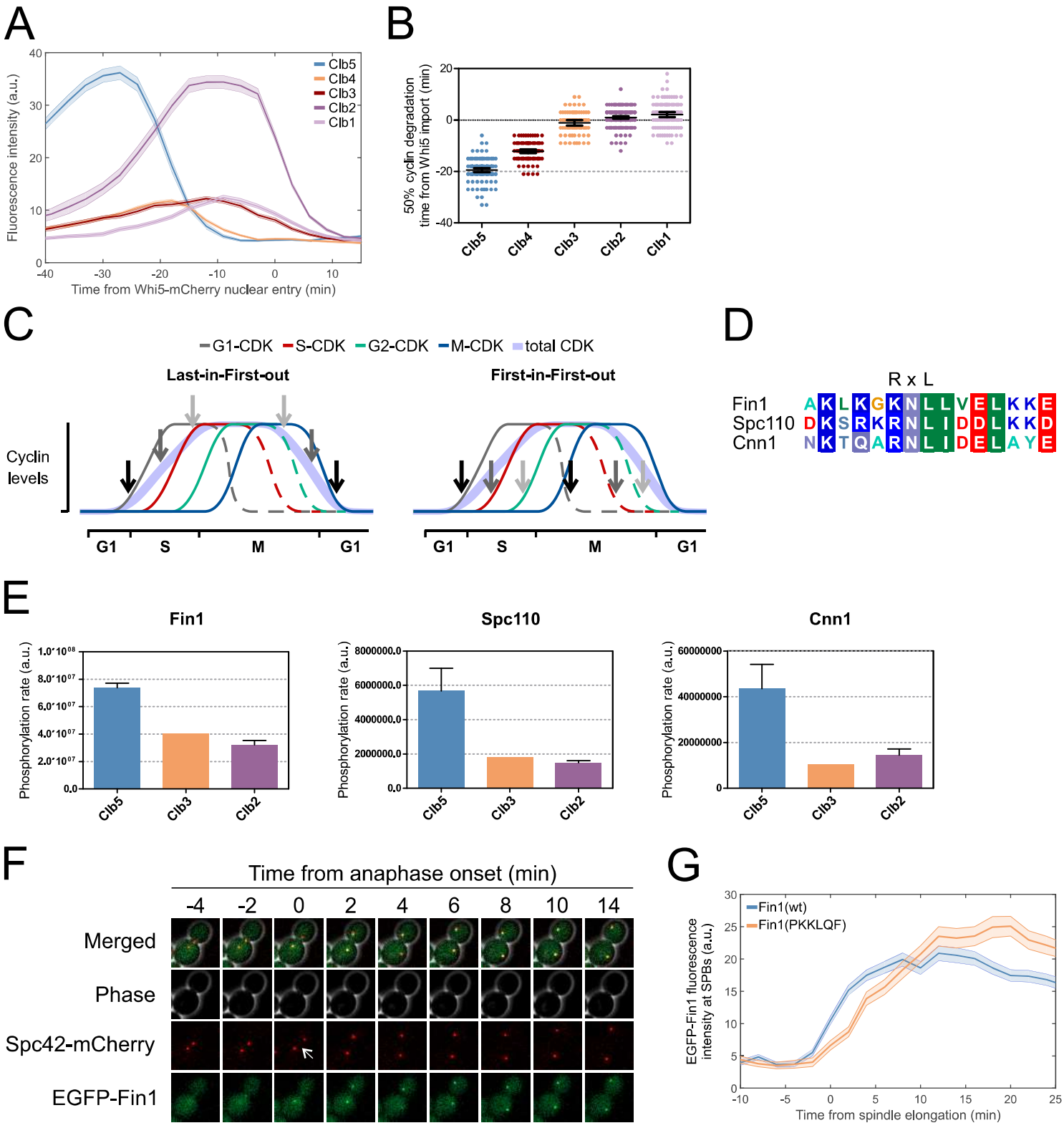

Figure 6. Exclusively Clb5-specific docking motifs improve substrate dephosphorylation in anaphase. (A) Time-lapse microscopy was used to measure cyclin-Citrine levels during mitotic exit in unperturbed cell cycles. The cells were synchronized by the nuclear import of 50% of Whi5-mCherry at mitotic exit. The plot shows mean ±SEM fluorescence intensities averaged over a population of cells. (B) Cyclin-Citrine degradation relative to the nuclear import of 50% Whi5-mCherry was followed in single cells. Plot shows the time from nuclear import of 50% Whi5-mCherry to the degradation of 50% of the indicated cyclin in individual cells. The error bars show 95% CI of the mean. (C) Simplified cell cycle model showing the expression profiles of 4 cyclins and the activation and inactivation of 3 CDK-dependent switches A, B, C. On the left plot, the switches are controlled in the last-in-first-out order and on the right, the first-in-first-out order. (D) Sequence alignment of predicted Clb5-specific RxL motifs in Fin1, Spc110 and Cnn1. (E) The effect of cyclin specificity on the phosphorylation of Fin1, Cnn1 and Spc110 was studied in a kinase assay. The plots show the phosphorylation by Cln2-, Clb5-, Clb3- and Clb2-Cdk1, the error bars show standard deviation. (F) Images from a time-lapse microscopy experiment of an exemplar cell expressing Spc42-mCherry for detection of SPBs and EGFP-Fin1. Cells were imaged every 2 minutes, the white arrow indicates onset of anaphase. (G) The accumulation of EGFP-Fin1 to SPBs in anaphase was measured in experiments described in 'F'. The plot shows mean EGFP fluorescence intensities at SPBs around the time of anaphase onset. The error bars are ±SEM.

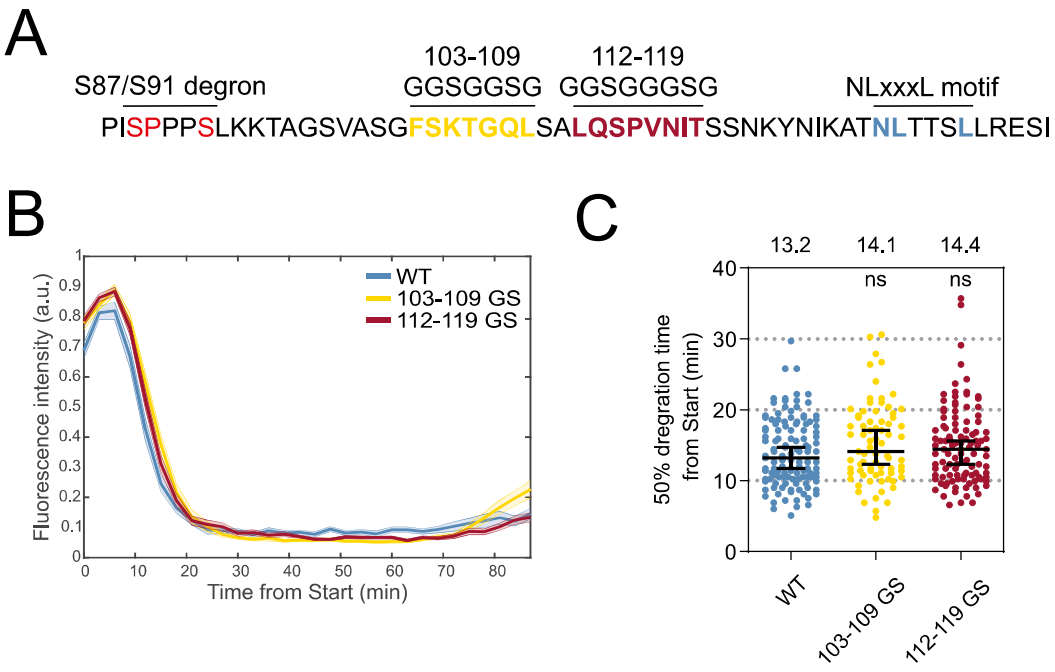

Supplementary Figure 1. Mapping of the NLxxxL motif. (A) Sequence of Far1 positions 85-140 showing th linker sequence between the S87/S91 degron and the NLxxxL motif. To study the linker region, positions 103-109 and 112-119 were replaced with glycine-serine linkers in two constructs that were analyzed in time-lapse microscopy in panel 'B'. (B) Mean±SEM fluorescence intensities of the indicated Far1(1-150)-GFP constructs after Start. (C) Plot showing the 50% degradation timing of indicated Far1(1-150)-GFP mutants in individual cells. The numbers above the plot show median values for each construct. ns denotes p-value > 0.05 for pair-wise comparisons with wild-type.

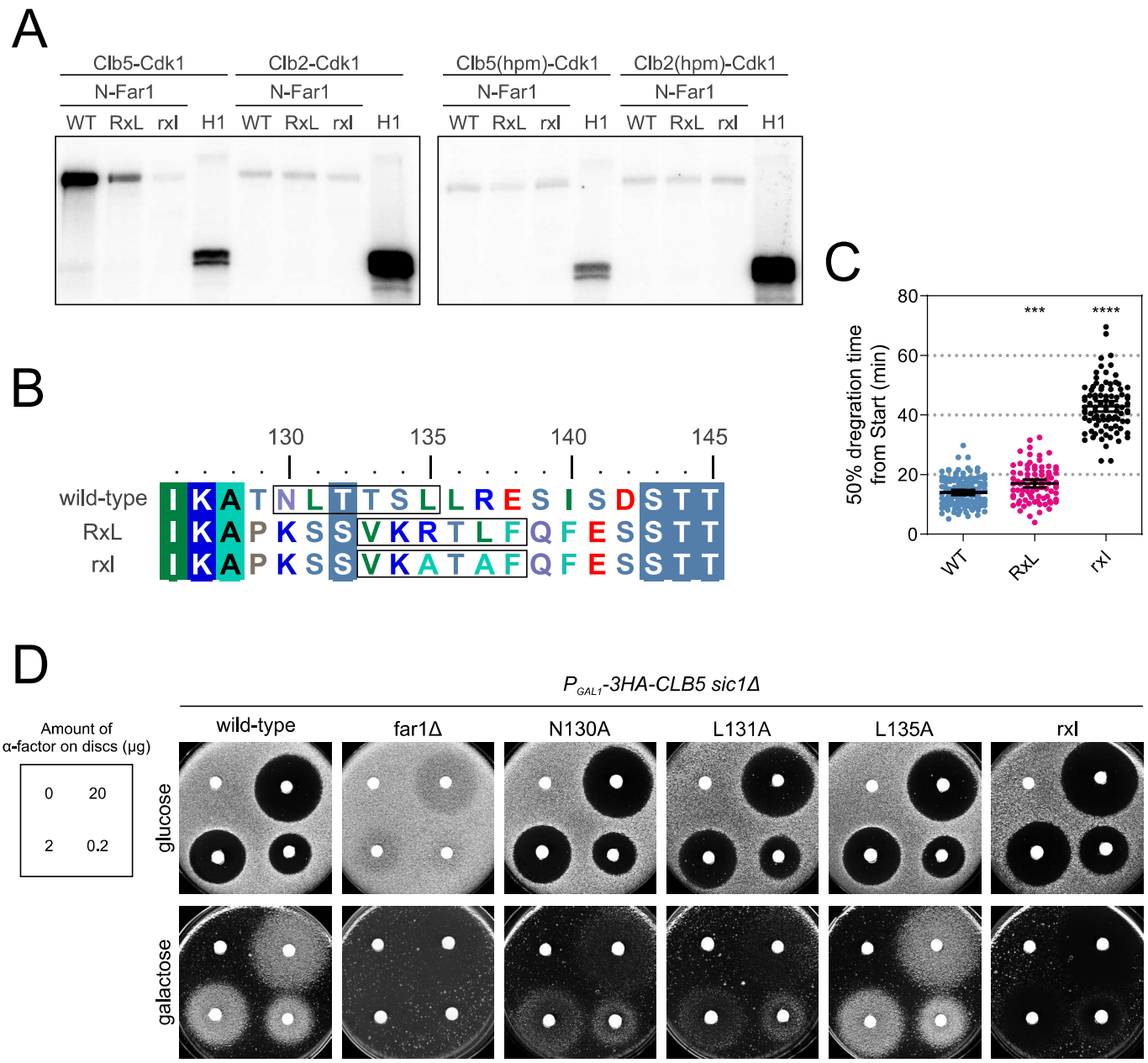

Supplementary Figure 2. Comparison of NLxxxL and RxL motifs in Far1. (A) Autoradiographs showing the Clb5-specificity and *hp*-dependency of phosphorylation of N-Far1 (Far1(1-150)-GFP) with either NLxxxL motif (WT), RxL motif (RxL) or mutated RxL motif (rxl). (B) Sequence alignment showing the introduction of wild-type or mutated RxL motif to Far1. (C) 50% degradation timings of the Far1(1-150)-GFP with either wild-type, RxL or mutated RxL docking motif in individual cells from time-lapse microscopy experiments. Error bars show median±95CI. **** and *** denote p-values <0.0001 and <0.001 for pair-wise comparisons with WT using Mann-Whitney U test. (D) Pheromone sensitivity halo assay in *sic1Δ* strains expressing the indicated *FAR1* variant. α-factor in different concetrations was pipetted on the paper discs as shown on the scheme. On galactose plates, Clb5 is expressed from P_{GAL1}, whereas on glucose plates, Clb5 expression is inhibited.

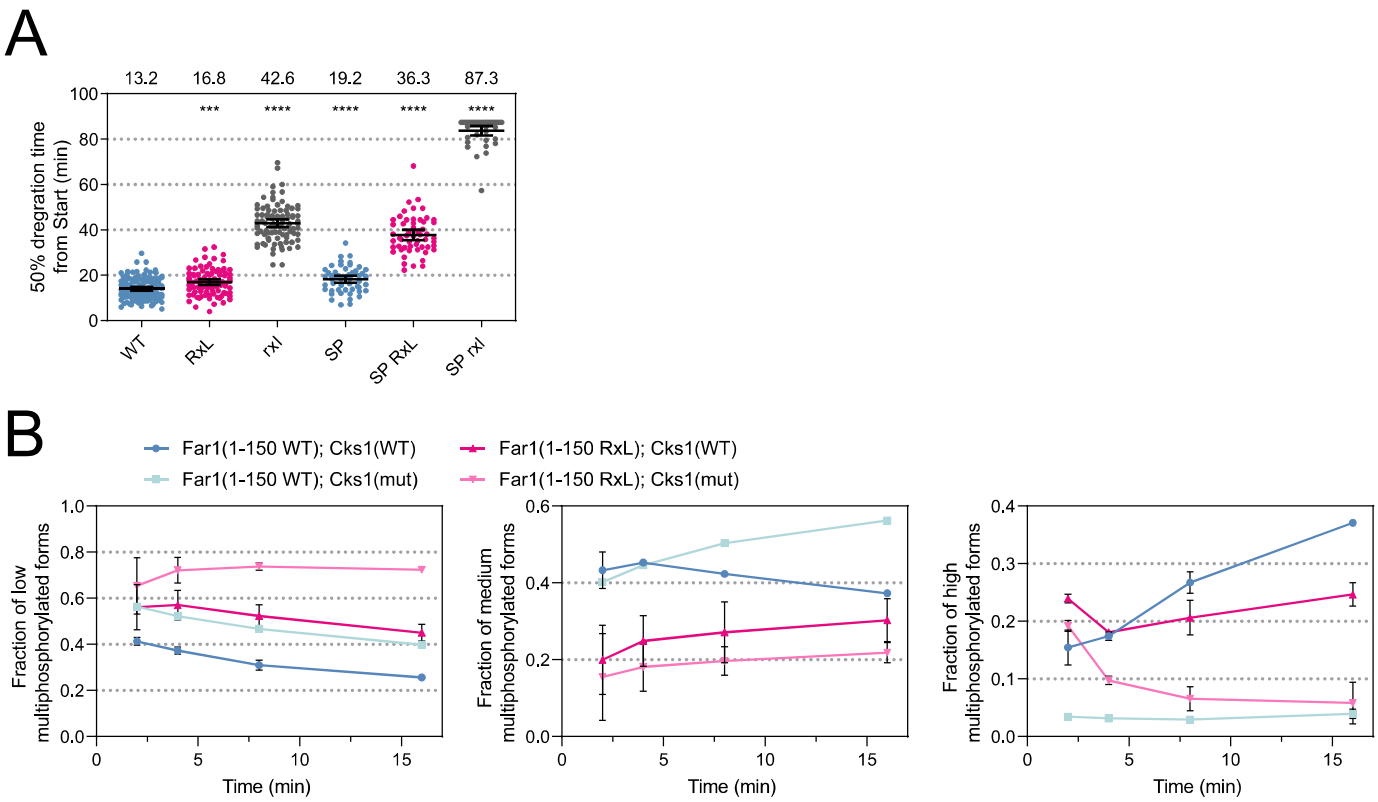

Supplementary Figure 3. The contribution of Cks1 to Far1 multiphosphorylation depends on the cyclin docking motif. (A) Plot showing the 50% degradation timing of the indicated Far1(1-150)-GFP mutant in single cells. Error bars show median ±95CI, **** and *** denote p-values <0.0001 and <0.001 for pair-wise comparisons with WT using Mann-Whitney U test. (B) Multisite phosphorylation of Far1(1-150)-GFP was studied in a kinase assay followed by Phos-tag SDS-PAGE. The different phosphorylated forms were quantified as shown in Fig. 3C. The plots show the fraction of differentially phosphorylated products during the reaction with either wild-type or RxL-containing substrate and wild-type or mutated Cks1.

A

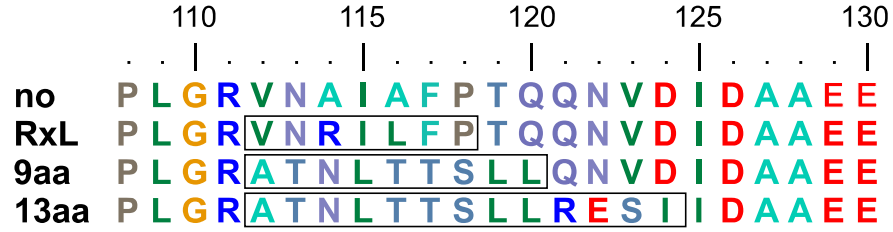

B

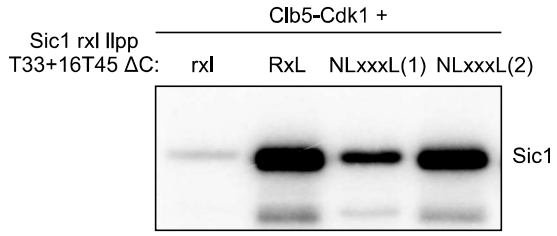

Supplementary Figure 4. NLxxxL is a linear and modular docking motif. (A) Alignment showing the mutation of Sic1 RxL motif and introduction of NLxxxL motif with different length of flanking sequences. (B) Autoradiograph of phosphorylation reactions of the indicated Sic1 variant and Clb5-Cdk1.

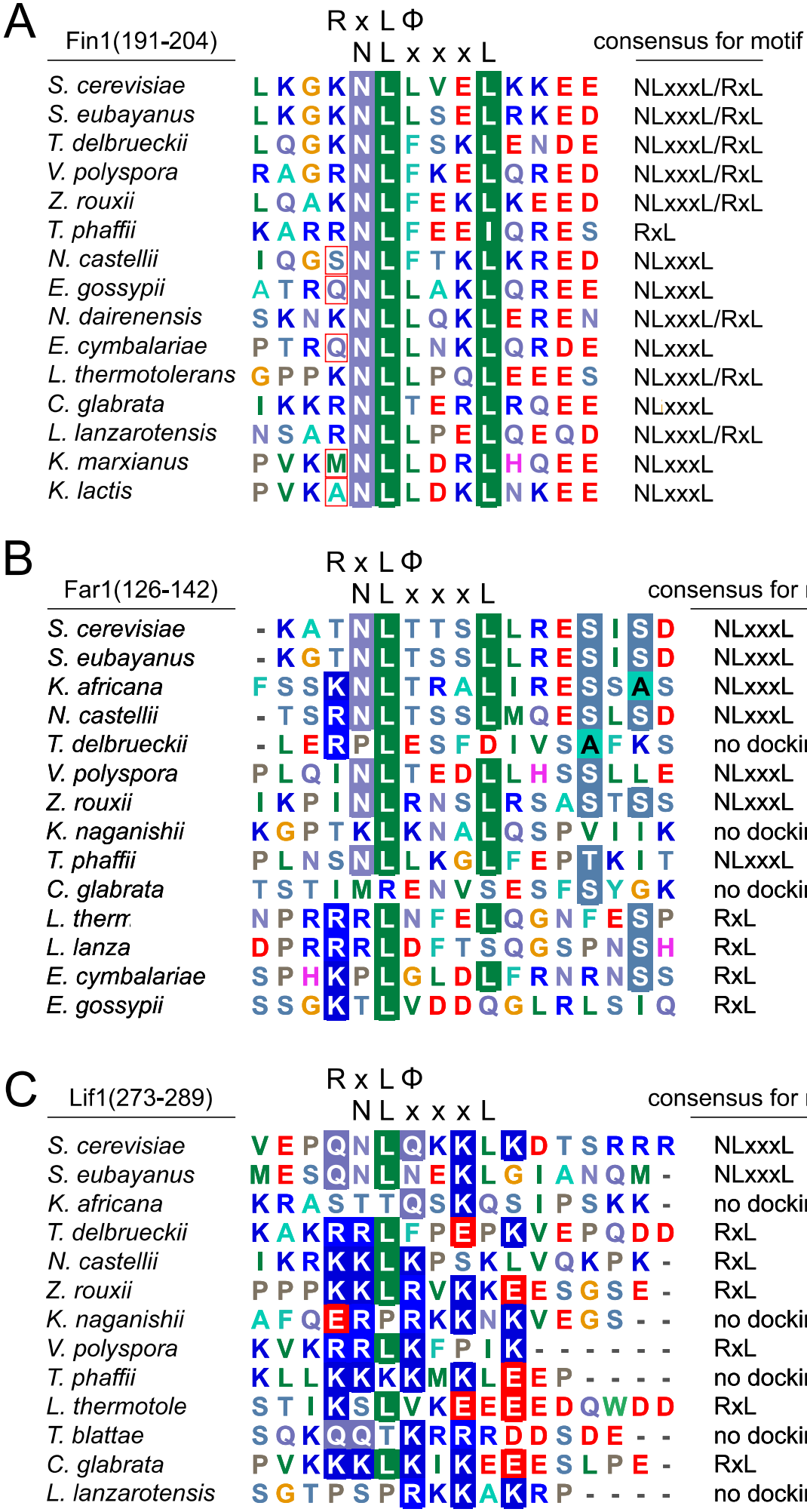

Supplementary Figure 5. Conservation of NLxxxL motifs in Fin1, Far1 and Lif1. (A-C) Alignment of Fin1 (A), Far1 (B) and Lif1 (C) homologs in yeasts showing the conservation and overlap of cyclin docking motifs. The match to either RxL or NLxxxL motif consensus is presented on the right. The RxL consensus was defined as R/K-x-L-Φ or R/K-x-L-x-Φ.

A

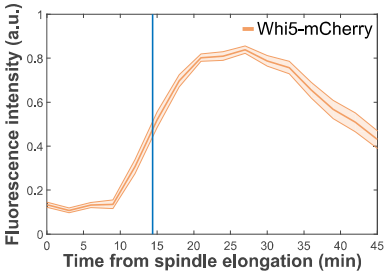

B

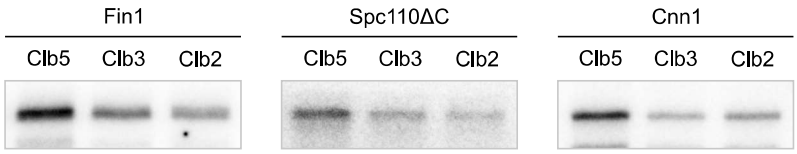

Supplementary Figure 6. Nuclear import of Whi5 and cyclin specificity analysis of Fin1, Spc110 and Cnn1 phosphorylation. (A) The nuclear fluorescence levels of Whi-mCherry after spindle elongation were measured in single cells using time-lapse microscopy. The plot shows mean levels from a group of cells synchronized at the time of anaphase onset detected by movement of Spc42-EGFP. (B) Cyclin specificity analysis of Fin1, Spc110 and Cnn1 phosphorylation. The indicated substrates were phosphorylated with Cln2-, Clb5-, Clb3- and Clb2-Cdk1 complexes, the reactions were stopped and separated by SDS-PAGE, the ^{32}P autoradiographs are shown.

Non-exclusive licence to reproduce thesis and make thesis public

I, Frida Matiyevskaya,

(*author's name*)

1. herewith grant the University of Tartu a free permit (non-exclusive licence) to:

1.1. reproduce, for the purpose of preservation, including for adding to the DSpace digital archives until the expiry of the term of copyright, and

1.2. make available to the public via the web environment of the University of Tartu, including via the DSpace digital archives, under the Creative Commons licence CC BY NC ND 3.0, which allows, by giving appropriate credit to the author, to reproduce, distribute the work and communicate it to the public, and prohibits the creation of derivative works and any commercial use of the work from ***20/05/2023*** until the expiry of the term of copyright,

S phase cyclin-CDK specificity in ordering cell cycle phosphorylation ,

(*title of thesis*)

supervised by PhD, Ilona Faustova and MSc, Mihkel Örd,

(*supervisor's name*)

2. I am aware of the fact that the author retains the rights specified in p. 1.

3. I certify that granting the non-exclusive licence does not infringe other persons' intellectual property rights or rights arising from the personal data protection legislation.

Frida Matiyevskaya

20/05/2020